TÉCNICO LISBOA

A GFPE Method To Estimate Noise Levels From Aircraft Departures At Montijo Aerodrome

Diogo Alexandre Neves Carreira Mendes

Thesis to obtain the Master of Science Degree in

Aerospace Engineering

Supervisor: Prof. João Manuel Gonçalves de Sousa Oliveira

Examination Committee

Chairperson: Prof. Fernando José Parracho Lau
Supervisor: Prof. João Manuel Gonçalves de Sousa Oliveira
Member of the Committee: Prof. Pedro da Graça Tavares Alvares Serrão

December 2020

'*What I cannot create,*
I do not understand.'
Richard Feynman

Acknowledgments

I would like to thank my family for providing support and encouragement along these years as well as for providing the best education to educate myself from now on. To my sister that put up with me all the time, for always been an excellent listener and for showing me the other side I would not see without her. To my uncle and aunt that never stopped pushing me to take an advanced engineering degree and for taking the possible and impossible to make it, while full filling me with their wisdom of living. To my mom, who gave me all the love that only a mother can give and apologized me for all my failures and mistakes. And finally to my father for his discipline and for preparing me to every battle further in life.

I would like to acknowledge my dissertation supervisor Prof. João Oliveira that has made this thesis possible. His insight, friendship and sharing of knowledge were the solid foundations of all my motivation during this long stage of developing a thesis where not always were clear for me that it would be possible. His patience and comprehension were important characteristics that distinguish him and I will never forget his role in my life.

To God Almighty, who is perfect in everyway, and who blessed me with the needed resilience along the most harsh times of my journey.

To every one of you,
Sincerely Thank You.

Abstract

In the past years, consciousness about health and environment are forcing each day to restrict the maximum allowed noise levels at the cities and big urban areas, leading to more accurate noise prediction tools that can include a much bigger number of parameters that influence the propagation itself as well as achieve a more complex propagation model with less computational demand and which is more user friendly, promoting this way that further developments can be made faster and better.

This dissertation starts by presenting the fundamentals of acoustic physics, and then a few existing numerical methods that predict the sound propagation in the atmosphere as well as its limitations.

The main goal of this thesis is to study the sound propagation in the atmosphere produced by an aircraft's departure and to use a numerical application which allows to incorporate the variations in the source position with some of the parameters that were used in the C language program which perform the calculations.

In order to achieve so, it was elaborated a Matlab script that generate the inputs of the executable and allows to obtain the noise levels for different situations of interest, accordingly to ANP database procedures for departure.

Keywords

sound propagation, SPL, GFPE, NPD, acoustic, noise, atmosphere.

Resumo

Nos últimos anos, a consciência sobre a saúde e o meio-ambiente está a forçar a cada dia que passa a restrição dos níveis máximos de ruído permitidos nas cidades e nas grandes áreas urbanas, levando a ferramentas de previsão de ruído mais precisas que podem incluir um número muito maior de parâmetros que influenciam a propagação e obter um modelo de propagação mais complexo, com menos exigência computacional e mais amigável para o usuário, promovendo que novos desenvolvimentos possam ser feitos de forma mais rápida e melhor.

Esta dissertação começa por apresentar os fundamentos físicos da acústica e de seguida alguns métodos numéricos existentes para a propagação do som na atmosfera, bem como suas limitações.

O objetivo principal deste trabalho é estudar a propagação do som na atmosfera, produzido por uma aeronave a descolar, através de um modelo numérico que permite incorporar a variação da posição da fonte em função dos parâmetros utilizados no programa escrito em linguagem C.

Para que o objectivo fosse cumprido foi elaborado um script em Matlab que gera os valores de input que posteriormente são corridos no executável e que permitem obter os valores de ruído para diferentes situações de interesse, e respeitando os procedimentos descritos na base de dados ANP.

Palavras Chave

propagação do som, SPL, GFPE, NPD, acústica, ruído, atmosfera.

Contents

List of Figures

Abbreviations & Symbols

Mathematical Notation

$d_x f$ - First partial derivative of function f in respect to x

$d_x^2 f$ - Second partial derivative of function f in respect to x

∇f - Gradient of a scalar function f

Abbreviations

AGL - Above Ground Level

AIP - Aeronautical Information Publication

AMSL - Above Mean Sea Level

CAS - Calibrated Air Speed

CNPE - Crank-Nicholson Parabolic Equation

dB - Decibel

dBA - A-weighted decibel

DTF - Discrete Fourier Transform

ECAC - European Civil Aviation Conference

FFP - Fast Field Program

FFT - Fast Fourier Transform

FFTW - Fastest Fourier Transform in the West

GFPE - Green's Function Parabolic Equation

ICAO - International Civil Aviation Organization

IFR - Instrument Flight Rules

ILS - Instrument Landing System

LPMT - Montijo Air Base

NPD - Noise Power Distance

PE - Parabolic Equation

RWY - Runway

SEL - Sound Exposure Level

SID - Standard Instrument Departure

SPL - Sound Pressure Level

STAR - Standard Terminal Arrival Route

STL - Sound Transmission Loss

TL - Transmission Loss

Roman Symbols

A - Attenuation factor

b - Parameter of logarithmic sound speed profile

c - Adiabatic sound speed

c_0 - Sound speed at the ground

c_{eff} - Effective sound speed

f - Frequency

g - Grain shape factor

k - Wave number

k_0 - Reference wave number at the ground

k_a - Reference wave number at a certain height

k_{abs} - Absorption layer wave number

k_{eff} - Effective wave number

L_A - A-weighted sound pressure level

L_{AE} - Sound exposure level

L_{Amax} - Maximum A-weighted sound pressure level

L_E - Single event sound exposure level

L_{max} - Maximum sound pressure level

L_P - Sound pressure level

$L_{P,free}$ - Sound pressure level of free field

M - Number of vertical points

n - Unit outward normal vector

N - Size of the Fourier transforms

N_{Pr} - Prandtl number

p_c - Complex pressure amplitude

p_{free} - Complex pressure of free field

p_{ref} - Reference pressure level

r - Horizontal distance

R - Distance from the source to the receiver

R_A - A-weighting filter

R_P - Plane wave reflection coefficient

s_f - Pore shape factor ratio

T - Absolute temperature

T_0 - Reference Temperature

u - Wind vector

u_r - Wind horizontal component

u_z - Wind vertical component

V - Integration Volume

z - Vertical coordinate

z_0 - Roughness length of ground surface

z_{abs} - height of the absorption layer

z_s - Source height

z_{top} - Height of the grid

Z_g - Acoustic impedance of ground surface

Greek Symbols

α - Atmospheric absorption coefficient

γ - Elevation angle

γ_{max} - Maximum elevation angle

δ - Diriac delta function

ΔL - Relative sound pressure level

Δr - Horizontal spacing

Δz - Vertical spacing

λ - Wavelength

ρ - Density of atmosphere

ρ_0 - Air density

σ - Flow resistivity of ground

Ω - Porosity of medium

Ψ - Fourier transform

ζ - Acoustic impedance

ζ_{air} - Acoustic impedance of air

ζ_g - Acoustic impedance of the ground surface

1

Introduction

1.1 Hystorical Background

It was long time ago that Aristotle correctly declared that sound consists of the propagation of air pressure variations. Fluctuations of pressure above and below the average pressure, arriving at the surface as sound, cause a very small increase or decrease respectively in the number of collisions per second, and a corresponding tiny measurable change of force on the surface. These fluctuations above and below the ambient pressure are called the pressure amplitude δP, where the total pressure is $P = P_0 + \delta P$ and P_0 is the ambient pressure [10]. Usually only the amplitudes matter to us and it's the changes in pressure that we hear, not the ambient pressure.

On the other hand humanity is living in a world with permanent contact with noise, remaining each day less places on Earth where we are totally free from undesirable sounds. Noise can frustrate and impede speech communication and it can represent a physical health hazard as well since the exposure to high noise levels can cause permanent hearing loss besides depression and anxiety. In the last years, society's growing environmental and health conscience has leaded the national authorities to reinforce existing legislation concerning the maximum permissible noise levels.

1.2 State of the Art

The most relevant existent methods to calculate the sound level in a given atmosphere are the Generalized Fast Field Program (FFP), the Crank-Nicholson Parabolic Equation (CNPE), the Ray Model method and the Green Function Parabolic Equation (GFPE).

FFP was originally developed as a computational method for underwater acoustics [11] and later adapted for outdoor sound propagation in the atmosphere. This computer model enables the prediction of sound pressure in a layered refracting atmosphere above an absorbing or rigid ground surface. The atmosphere is divided in horizontal homogenous layers where each one has its own wave number and the wind speed and temperature are constant. The sound field is computed in the horizontal wave number domain and requires a Fourier transformation of the used wave equation, from the horizontal spatial domain to the wave number domain. This is necessary to solve numerically the wave equation. Thereafter, an inverse Fourier transform is used to obtain the sound field in the spatial domain, back from the horizontal wave number domain. Only one frequency is obtained per sound field calculation which makes computing an entire frequency spectrum very time consuming.

CNPE is based in an approximation of the wave number equation, which, in this case, can be either a narrow-angle $(< 15^\circ)$ or a wide-angle parabolic equation $(< 35^\circ)$. The parabolic equation is solved numerically by approximating the wave equation derivatives by a two dimensional finite difference Crank-Nicholson scheme. Since the grid spacing varies with the source frequency, the number of

extrapolation steps required can be very high for very high frequencies or for large distances, requiring a lot of computational effort and time to calcuate the sound field.

The Ray model, also called geometrical acoustics, consists in calculate the paths of all rays between the source and the receiver as well as the sound pressure given by the contribution of all those rays. The number of rays increases with the distance between the source and the receiver thus making this model less suitable for long range sound propagation. The calculation of all ray paths also requires a computational algorithm to map all ray paths, from the source to the receiver making this model less attractive for calculations of outdoor sound propagation.

The GFPE model uses a Green function which is applied to solve the inhomogeneous wave equation, in a rectangular grid like the one used in CNPE. The sound field is computed in the vertical wave number domain, so two Fourier transforms are used. The first one transforms the spatial domain into the vertical wave number domain, while the second one changes back to the spatial domain. This method analytically takes into account the horizontal wave oscillations in the field, which allows larger horizontal extrapolation steps up to 50 wavelenghts [12]. These characteristics make the GFPE method the appropriate choice for an atmospheric computational program, combining the superior real atmosphere modeling of the PE method, with the faster long range calculations of the FFP method.

1.3 Motivation

In view of the described context, the knowledge of the sound propagation assumes a growing importance. Nowadays all the previous studies associated with the construction of new infrastructures or the renewing of another ones, that can generate significant levels of noise, namely airports, involves the need for countless studies, which take into account an incredible amount of parameters in order to achieve precise results. In this scope, there has been a continuous effort to decrease aircraft noise emissions through specified planning of procedures for the flight paths allowed in the vinicity of airports.

As proven [1] [4] [13], the Green Function Parabolic Equation method is the most suitable method to study sound propagation in the atmosphere. Using this method, it was developed in previous studies a computational program in C language to calculate the sound field between a source and a receiver, where it's included several inputs that represent the most significant parameters of sound propagation phenomena. This method puts together the best accuracy and computational effort of each of the existing methods and its results were validated by comparison to well known benchmark results.

Finally, in order to apply the sound propagation to a real case scenario, it was developed a Matlab program in which is calculated an aircraft departure trajectory following the ECAC Vol.II procedures in order to discretize a departure flight path for the Montijo's airbase.

1.4 Outline

This chapter presents a brief summary and description of the objectives of this dissertation.

Chapter 2 describes the theoretical fundamentals and definitions related with sound propagation in the atmosphere, as well as some of the main parameters that influence its physics depending on the type of atmosphere and its conditions. Two main types of different atmosphere are approached being the homogeneous and inhomogeneous respectively.

Chapter 3 details the propagation model as a method to solve the inhomogeneous Helmholtz equation through out its discretization. It's approached the fundamentals that support all the further computational implementation developed. In the end of this chapter it is briefly revised and approached a more recent formulation called EWAPE which accounts to wider angles in atmospheric sound propagation by using the GFPE method.

Chapter 4 presents and explains the assumptions used in the developed C language program which calculate the sound field between the source and the receiver. This program incorporates the main parameters that govern sound propagation as for example the ground impedance and the range, in a designed atmosphere. It also validates the GFPE formulation by comparison with existing benchmark results for atmosphere sound propagation problems well known.

Chapter 5 presents the ECAC Vol.II noise model, starting by the definition of the coordinate systems, followed by the concept of flight path segmentation and the general expressions for calculating noise levels during a takeoff operation, based on empirical tabulated data. The trajectories projected were based in the NAV-Portugal studys for the Montijo's airport which account the overflight of the natural reserve located in Ponta da Erva.

Chapter 6 reveals the several restrictions and specifications of the Montijo's airbase and it is presented the chosen flight path that was taken into account for the simulations. Three main trajectories were designed varying on the turning radius and finally the noise levels at the observer were obtained.

Chapter 7 provides a general discussion and concluding remarks of the present work, as well as, a few suggestions of interest for future developments.

2

Theoretical Fundamentals

This chapter is a review of the most important concepts and mechanisms that control sound propagation in the atmosphere. Since the field is so vast, only the dominant mechanisms of sound propagation will be presented here. Section 2.1 gives a general view over the atmospheric acoustics and its physics, while sound propagation in a homogeneous atmosphere (section 2.2) and sound propagation in an inhomogeneous atmosphere (section 2.3) are the following two areas described in this chapter.

2.1 Atmospheric Acoustics

2.1.1 Noise Physics

Sound is a mechanical wave, which is an oscillation of pressure transmitted through a medium, composed of frequencies within the range of hearing and with a level sufficiently strong to be felt by human eardrums and that ultimately results in listening. A sound propagation scheme is illustrated below by a source, located at a given height Z_s above the ground, and a receiver, at a distance from the source R and placed at a certain height Z_r.

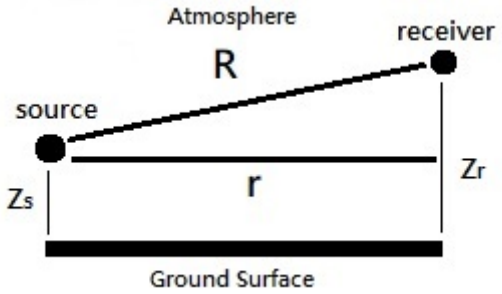

Figure 2.1: Sound propagation geometry

Sound pressure in a atmosphere is the local pressure deviation from the average atmospheric pressure caused by a sound wave. The sound pressure level (SPL) is a logarithmic measure of the effective sound pressure of a sound relative to a reference value. Its value is measured in decibel and is given by the following equation 2.1

$$L_P = 10log_{10}\left(\frac{1}{2}\frac{|p_c^2|}{p_{ref}^2}\right) \tag{2.1}$$

where P_{ref} is a reference value of $2\times10^{-5}Pa$ for the threshold of human hearing and P_c is the sound pressure of a harmonic spherical wave.

It is also useful to define another quantities such as the relative sound pressure level L_p and sound pressure in a homogeneous atmosphere without ground surface, given by the following expressions:

$$\Delta L = L_P - L_p, free \tag{2.2}$$

$$L_p, free = 10log_{10}\frac{1}{2}(\frac{|p_{free}|^2}{p_{ref}^2}) \tag{2.3}$$

From this two shown expressions, we can obtain a new relative sound pressure level formula which will be used further ahead to characterize the noise levels by the developed program:

$$\Delta L = 10log_{10}\frac{1}{2}\frac{|p_c|^2}{|p_{free}|^2} \tag{2.4}$$

Last but not least, it is important to define another parameter called Sound Transmission Loss [14] which is a quantification in decibels of how much energy is prevented from traveling through a medium. From an engineering application point of view it is useful for benchmarking and comparison purposes.

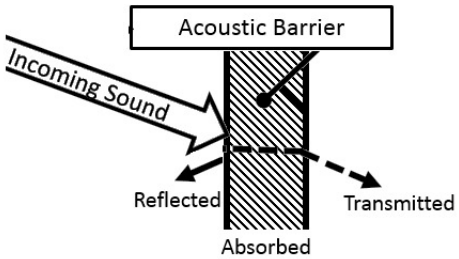

Figure 2.2: Sound Transmission Loss illustration

The source is characterized by the free field pressure which is the sound pressure of the source in an unbounded homogeneous atmosphere.

From a more practical perspective, STL can be understood as the ratio of the acoustic energy transmitted versus the amount of acoustic energy on the incident side of the material and mostly depends on the treatment material and frequency of the incoming sound. Its mathematical expression can be written as follow:

$$STL = 10log_{10}\frac{|p_c|^2}{|p_{free}|^2_{r=1}} \tag{2.5}$$

Where $|p_{free}|^2_{r=1}$ is the sound pressure from a direct acoustic field at 1 meter from the source.

2.1.2 Noise Metrics

The quantities defined in the previous section allow the determination of the sound field in terms of sound pressure level emanating from a monopole source defined by a power spectrum. However, when studying aviation noise, this quantity is not sufficient since the main goal is to study the effect of aircraft operations in the surrounding populations. Therefore the numerical models must include algorithms that rewrite the noise data in terms of human perception.

The first main characteristic of human perception that can be modeled is the different sensitivity of the human ear in the audible frequency spectrum. This phenomenon can be studied using two different scales: the A-weighted sound level and the Tone-corrected Perceived Noise Level. The A-weighting scale consists on a simple filter that applies more or less emphasis to certain frequencies to mirror the human ear sensitivity. This scale is applied in almost every sound application and the A-weighted levels are normally defined as L_A. The mathematical definition of the sound filter defined in this paragraph is exposed below,

$$L_A(f) = L_P(f) + 20log_{10}\frac{R_A(f)}{R_A(1000)} \tag{2.6}$$

Where $R_A(f)$ is given by

$$R_A(f) = \frac{12200^2 f^4}{(f^2+20.6^2)(f^2+12200^2)(f^2+107.7^2)^{1/2}(f^2+737.9^2)^{1/2}} \tag{2.7}$$

The tone-corrected perceived noise levels are mainly used for precision aircraft noise measurements and model the human perception of noise from sources consisting of pure tones or other spectral irregularities. As this frequency weighting scale is computed by a complex procedure, as established by the International Civil Aviation Organization [5], it is not modeled in the program developed in this thesis because it is not possible to know or predict the complex tone of a moving aircraft.

The second characteristic of human perception that must be taken into account when studying aircraft noise is related to the exposure to a certain noise event and it is denominated noise metrics. There are two main categories regarding noise metrics: the first describing the single noise events (Single Event Noise Metrics) and the other considering the effects of longer exposure intervals (Cumulative Noise Metrics). The latter index, a measure of community annoyance, will not be approached in this dissertation as it is related to multiple aircraft movements, therefore does not lie within the scope of this research.

The previous presented equations are used to model outdoor sound propagation and are valid to harmonic sources which have only one frequency. In practice, most of generated sounds are the result of several coupled harmonics and therefore, in order to model, for example, an aircraft noise is necessary

to decompose the sound in several harmonics. This can be mathematically represented by,

$$p(t) = \sum p_f(t) \tag{2.8}$$

Where $p_f(t)$ are the several harmonic pressure of the source frequency spectrum.

In chapter 6, the results of noise level presented are the Overall Sound Pressure Levels (OASPL) which are calculated by the following expression

$$L_P = 10log_{10}(\sum 10^{\frac{L_p(f)}{10}}) \tag{2.9}$$

For a source containing a large number of harmonic contributions the previous calculations can be very time consuming and therefore one typically replaces the values of each individual frequency by a smaller normalized number of $1/3$ octave bands which have discretized values as shown below.

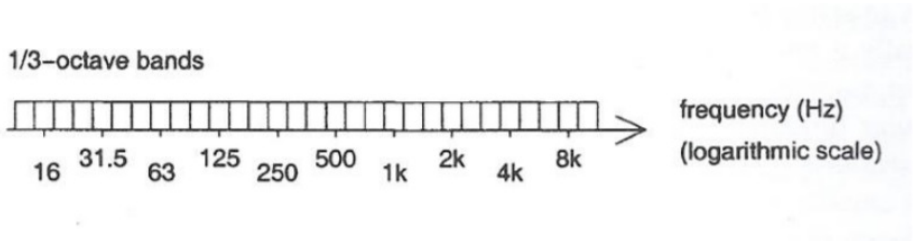

Figure 2.3: $1/3$ octave band frequency scale [1]

This allows to simplify the study of a sound field produced by a non harmonic source by limiting the number of harmonic frequencies to a representative group. This bands are also characterized by a center, a lower and an upper frequency which can be calculated by the next three expressions respectively,

$$f_{center} = 1000 \times 2^{-10+m/3}[Hz] \tag{2.10}$$

$$f_{lower} = f_{center} \times 2^{-1/2}[Hz] \tag{2.11}$$

$$f_{upper} = f_{center} \times 2^{1/2}[Hz] \tag{2.12}$$

Where $m = 1, 2, 3, ...$

2.2 Homogeneous Atmosphere Acoustics

In a homogeneous atmosphere with no wind, boundaries or surfaces, sound propagation is strictly axisymmetric and there is no angle dependence.
It's also assumed that average density and pressure remain constant and therefore the sound wave propagation is influenced by three main cases that will be further discussed in this section being repectively the acoustic spreading, the atmospheric absorption and the ground absorption.

2.2.1 Acoustic Spreading

The sound wave travels from a source and spread along a surface of increasing radius,where the sound intensity decreases as the surface of the wave front expands. The resulting dissipation is dependent on the propagation distance and independent of frequency.

For a point source, the spreading is spherical and the sound level decreases 6 dB per each doubling distance.

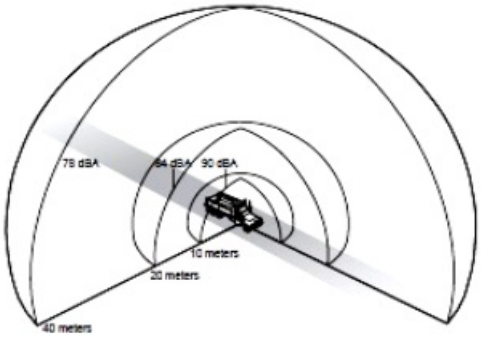

Figure 2.4: Spherical spreading [2]

The sound emitted by an airplane or car can be considered as a point source, thus the spreading is spherical as shown above. On the other hand, a busy highway can be comparable to a line source with cylindrical spreading. Assuming an infinite line source, the spreading of the sound waves is cylindrical and the sound level drops 3 dB per each doubling distance.

There is another interesting phenomena which is the sound generated by a source in mid-ocean that can not continue to spread uniformly in all directions once it reaches the sea floor. From that moment onwards, sound is trapped between the boundaries of the ocean and it gradually spreads cylindrically, with sound radiating horizontally away from the source. Sound levels decrease more slowly as sound

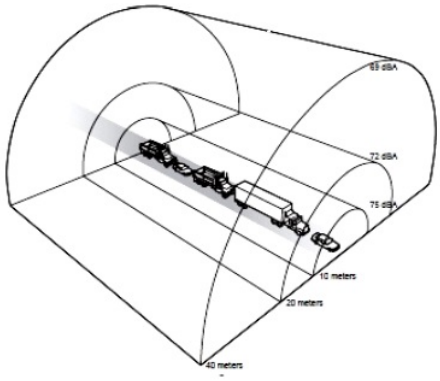

Figure 2.5: Cylindrical spreading [2]

spreads from a cylinder with a small to a larger radius, compared with the rate of decrease for spherical spreading [2].

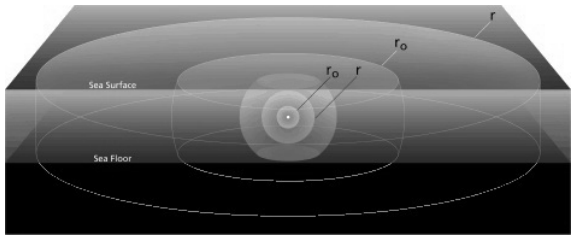

Figure 2.6: Spherical and Cylindrical spreading in mid-ocean [2]

Due to this spherical and cylindrical spreading, noise from point sources becomes quieter with each doubling of distance. When the sound source region is large compared to the distance to the listener's position, sound levels decrease more gradually and in typical urban settings, where setback distances are limited, geometric spreading generally accounts for most of the natural sound attenuation between noise sources and receivers. Spreading losses represent only a reduction in the sound power per unit area as the distance of an expanding wave front increases.

2.2.2 Atmospheric Aborption

As sound waves pass through the atmosphere, they lose energy in a gradual process that depends on air temperature, humidity and also atmospheric pressure.

Atmospheric absorption has little impact over the limited source-to-receiver distances typically experienced in the city. However for distances of 100 or more meters, it can begin to reduce overall noise levels as well as alter the character of complex sounds. This is because air absorption attenuates high frequency components faster than low frequency ones and this is why the sound from distant traffic or jets usually have a low rumbling character.

The real loss of sound power from the noise source is called atmospheric absorption and results mainly from a combination of three parameters:

1- Thermal conduction and viscosity of air

2- Vibrational relaxation of air molecules

3- Rotational relaxation of air molecules

This loss exists due to simultaneous small amounts of heating, viscous losses and energy exchange between air molecules, as a sound wave passes through. In this process the sound wave loses energy which is converted into heat.

In the following figure, the atmospheric absorption coefficient is displayed in a frequency domain, assuming a temperature of 20º, 70% of relative humidity and a pressure of 1 atm.

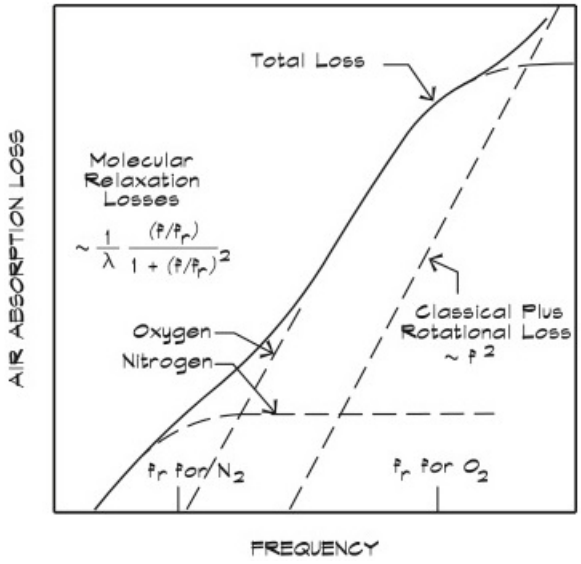

Figure 2.7: Absorption coefficient in dB/100m as a function of frequency f [3]

The vibration losses for O_2 and N_2 molecules are influenced by the presence of water vapor in the air because a vibrational energy exchange is more likely for a collision between H_2O and these two other molecules. Consequently, water vapor catalyzes the transfer of energy between the modes and reduces the vibrational relaxation time. Large concert halls must be designed to control not only temperature but also humidity since dry air can result in considerable loss of high-frequency energy.

2.2.3 Ground Effect

For most of outdoor sound propagation situations, there is a third source of natural noise attenuation that occurs when sound waves are bounded by any kind of ground surfaces and it is called Ground Effect. The proximity to a ground surface results in a complex interaction between the sound waves causing local cancellation of direct and ground-reflected sound waves [15].

An idealized scenario to give a clear understanding of this effect is where the listener is separated from a busy roadway by a wide, flat stretch of soft terrain. The ground effect can render noise from this roadway virtually inaudible to other receivers. Even at smaller distances across urban areas, as boulevards, the effect can be significant for receivers near ground level. Considering this effect, it is advantageous to install soft surfaces as flower beds or gardens as a way to reduce noise, and this is translated in much better life conditions for a residential area near noisy sources.

Considering an aircraft flying situation, besides it is not bounded by any ground surfaces, there are still sound waves that reach the ground, where part of each is reflected to the air and other part absorbed by the ground.

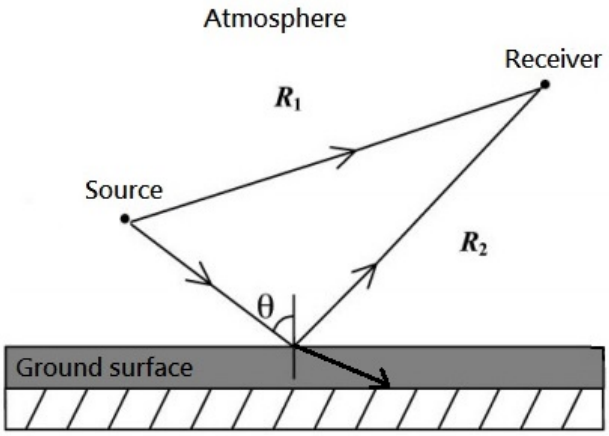

Figure 2.8: Sound propagation above a ground surface [4]

In figure 2.8 it's shown the direct wave R_1 and the reflected wave R_2. If both source and receiver are not in a too low position, the wave reflection coefficient R_p can be approximated as for the case of plane waves and it is presented in equation 2.13.

The plane wave reflection coefficient is given by expression 2.14 which depends on the angle of incidence θ and Z_g which is the ground impedance, a complex number defined as $Z_g = \frac{\xi_g}{\xi_{air}}$. The acoustic impedance ξ, is the ratio of the complex pressure and the amplitude of an acoustic wave trav-

eling through a medium. For an acoustically hard surface, like water or concrete, the ground impedance tends to infinity and on the other hand, an acoustically absorbing ground, like grassland, has a finite value of ground impedance.

$$R_p = \frac{Z_g cos(\theta) - 1}{Z_g cos(\theta) + 1} \tag{2.13}$$

$$\xi = \frac{p_c}{v_c} \tag{2.14}$$

2.3 Inhomogeneous Atmosphere Acoustics

2.3.1 Atmospheric Refraction

Acoustical propagation direction is largely affected by wind gradients as well as temperature gradients. Regarding wind effect, when it blows from the receiver to the source direction, it makes the sound waves to bend upwards from the ground. This create a zone of quiet at large distances, and this zone it is called sound shadow. When the wind blows in the same direction as the sound, sound waves are bended downwards, which can increase significantly the level of noise reaching distant receivers.

Regarding temperature gradients, they produce similar bending effects. During daytime conditions, when usually air is warmer near the ground, sound is bent upwards away from the ground which under calm conditions may cause sounds shadows in all directions from the source. Sound waves also propagates faster than sound travelling more distant of the ground. Due to this both factors, maintaining a distance from the source of sound would result in considerable sound attenuation. This change of the sound wave propagation is called atmospheric refraction and for distances shorter than 100m can be ignored. However, since most of outdoor propagation problems deal with long range propagation, the wind and temperature effects are usually significant, and also more common.

In this thesis it will be incorporated the effect of atmospheric refraction, which means that the sound speed in the atmosphere depends on temperature, where higher temperature yields faster sound propagation. The sound speed expression is presented below.

$$c = c_0 \sqrt{\frac{T}{T_0}} \tag{2.15}$$

In the presented expression, T is the temperature in Kelvin, c_0 is the sound speed at the temperature T_0. The standard values are $c_0 = 343m/s$ and $T_0 = 293$.

Refraction caused by temperature is the same in all directions since it is a scalar quantity. However the refraction caused by wind depends on the sound propagation, which can be represented by a vector of two coordinates $u(r, z) = (u_r, u_z)$ assuming a cylindrical coordinate system.

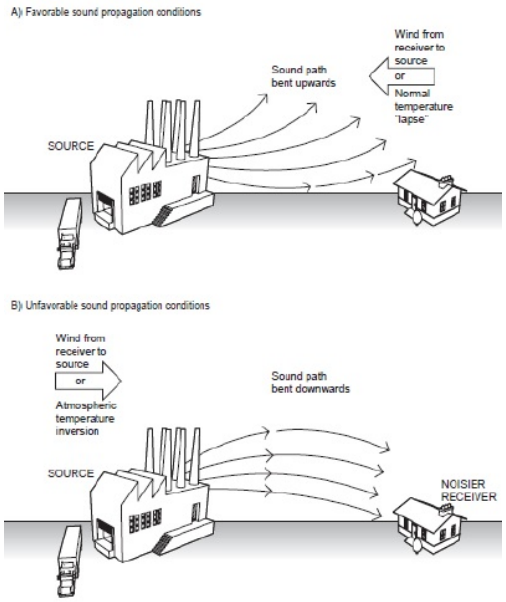

Figure 2.9: Effects of wind and temperature gradient on sound propagation [3]

When the sound propagates perpendicular to the wind path, the refraction caused by wind is neglected [1]. Therefore we can approximate a moving atmosphere to a non-moving atmosphere using an effective sound speed given by the following equation.

$$c_{eff} = c + u_r \tag{2.16}$$

where c is the adiabatic sound speed and u_r is the component of the wind speed in the direction of sound propagation. If the wind blows in the opposite direction to sound propagation, it has a negative contribution to the sound speed and the sound rays are bent away from the ground, resulting in upward refraction. A more realistic approach takes into account that wind speed near the ground is approximately zero and therefore it's often used a logarithmic function to describe the effective sound speed:

$$c_{eff} = c_0 + b\ln((\frac{z}{z_0}) + 1) \tag{2.17}$$

In the presented expression c_0 is the sound speed at the ground surface, the parameter z_0 is the roughness length and b is the refraction velocity, which is positive for downward bending and is negative for upward.

2.3.2 Atmospheric Turbulence

In the previous section, the atmosphere was characterized by vertical profiles of both temperature and wind. These profiles were assumed to be average values over a period of time, typical over 10 minutes. However, in a real atmosphere, the profiles change continuously. These fluctuations can occur in a scale of several hours or longer, but also occur in much faster scales, of seconds or minutes. The latter fluctuations are known as atmospheric turbulence.

Two types of flow exist in fluid dynamics: laminar and turbulent. Laminar flow occurs when a fluid travels smoothly or in regular paths, without any disruption between them. This type of flow is the least common in most aerodynamics problems, and is usually present in low velocity flow or when the flow section is relatively small. If the flow speed increases, the fluid transits into a new state characterized by chaotic and stochastic property changes, called turbulent flow.

Due to its complexity and associated computational effort, the incorporation of atmospheric turbulence was not in the scope of this thesis.

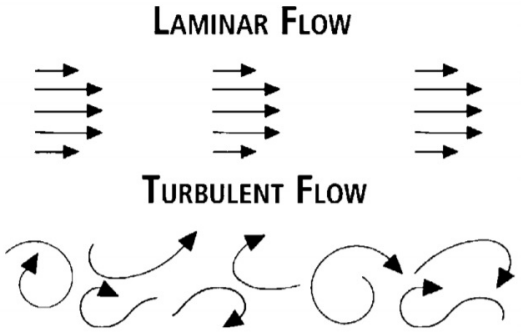

Figure 2.10: Illustration of laminar and turbulent flow [4]

3

Propagation Model

3.1 Parabolic Equation Method

The Parabolic Equation (PE) method is a computational model based on a parabolic equation and it is a step by step solution that uses a two dimensional grid where the source is at an arbitrary vertical position, and sequentially solves the respective parabolic wave equation.

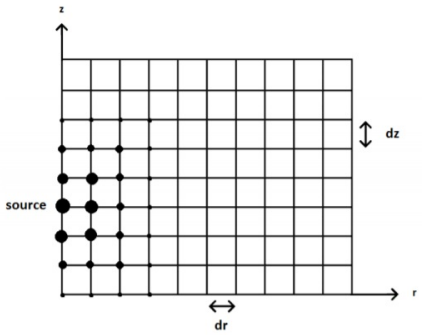

Figure 3.1: Grid used in the two dimensional PE models [1]

The solution is usually computed in two dimensions and it uses an axisymmetric approximation. With this method, it is possible to change the sound speed gradient and the ground impedance along the route of propagation thus, it is also possible to include range dependent atmospheric conditions. There are different types of parabolic equations, each of them having a specific maximum elevation angle γ_{max}, thus, the sounds levels are only valid for receivers with elevation angles smaller than a specific value [16].

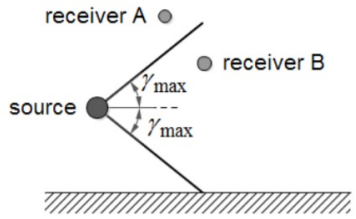

Figure 3.2: Angular limitation of the PE method [1]

In Figure 3.2, the receiver A is outside the area defined by the maximum angle so the results are not accurate, while on the other hand, the receiver B is inside this area, where the sound levels are valid.

For most outdoor sound propagation problems, both the source and the receiver are close to the ground, or the distance between them is large enough to minimize the influence of this limitation. The parabolic equation is a one-way wave equation, thus the sound from a source is always directed outwards. This results in the absence of back scattering of sound waves but, as the sound speed profiles are commonly a smooth function of position, sound waves travel mostly from the source to the receiver.

There are two major methods for solving the parabolic equation approached in this thesis:

- The Crank-Nicholson Parabolic equation (CNPE) method.
- The Green's Function Parabolic equation (GFPE) method.

In the scope of the main goals of this thesis, GFPE method was the used numerical method to solve the parabolic equation since it is fast and has good accuracy.

3.2 Green's Function Parabolic Equation Method

We will start by providing a brief theoretical background of the Green's Function Parabolic Equation method, both in a homogeneous and inhomogeneous atmosphere above a ground surface. The remainder of the chapter is oriented to the details involved in the numerical implementation of such propagation model.

3.2.1 Inhomogeneous Helmholtz equation

The propagation model derived in this chapter is based on linear acoustics, which considers that the pressure variations created by a sound wave are small when compared with the average pressure in the surrounding environment. This assumption allows the elimination of the nonlinear terms that are only necessary when studying very loud sounds such as the sound of an explosion [1].

Considering a monopole source in a moving atmosphere with a non constant sound speed profile, the corresponding three dimensional Helmholtz equation is

$$k_{eff}^2 \nabla.(k_{eff}^{-2}.p_c) + k_{eff}^2 \nabla p_c = 0 \tag{3.1}$$

where $p_c(\mathbf{R})$ is the complex pressure amplitude, $\mathbf{R}$ is a position vector and k_{eff} is the effective wave number, defined as

$$k_{eff} = \frac{w}{c_{eff}} \tag{3.2}$$

where w is the angular frequency of the sound wave and c_{eff} is the effective sound speed as previously described.

As the majority of sound propagation models is based on a two-dimensional atmosphere, further simplifications may be applied to the three dimensional Helmholtz equation.

Using a cylindrical coordinate system (r, ϕ, z), ϕ the azimuthal angle and r and z are consistent with Figure 3.1, we can now be write the following equation,

$$\frac{1}{r}\frac{d}{dr}(r\frac{dp_c}{dr}) + k_{eff}^2 \frac{d}{dz}(k_{eff}^{-2}\frac{dp_c}{dz}) + \frac{1}{r^2}\frac{d^2 p_c}{d\phi^2} + k_{eff}^2 p_c = 0 \tag{3.3}$$

In the axisymmetric simplification we consider that the sound field is independent of the azimuthal angle and therefore we can neglect the third term on the left-hand side of the previous equation. Replacing p_c by the quantity

$$q_c = p_c\sqrt{r} \tag{3.4}$$

and assuming only the far-field approximation, the resulting equation is

$$\frac{d^2 q_c}{dr^2} + k_{eff}^2 \frac{d}{dz}(k_{eff}^{-2}\frac{dq_c}{dz}) + k_{eff}^2 q_c = 0 \tag{3.5}$$

For most numerical applications, the second term of previous equation can be approximated by [1]

$$k_{eff}^2 \frac{d}{dz}(k_{eff}^{-2}\frac{dq_c}{dz}) \approx \frac{d^2 q_c}{dz^2} \tag{3.6}$$

Replacing k_{eff} by k and q_c by q , equation 3.5 becomes

$$\frac{d^2 q}{dr^2} + \frac{d^2 q}{dz^2} + k^2 q = 0 \tag{3.7}$$

where $q = q(r, z)$ and $k = k(z)$.

This last equation is the basis for the derivation of the GFPE propagation model.

3.2.2 Kirchhoff-Helmholtz integral equation

Considering now a volume V occupied by an inhomogeneous fluid and enclosed by a surface S with an outward normal vector **n**, it can be shown that the complex pressure amplitude $p(\mathbf{R_A})$ at a point $\mathbf{R_A} = (x_1, y_1, z_1)$ can be calculated by employing the Kirchhoff-Helmholtz integral equation. Therefore, it states that if the sound pressure is determined in all points on its surface, the sound pressure inside the volume free of sources can be also calculated.

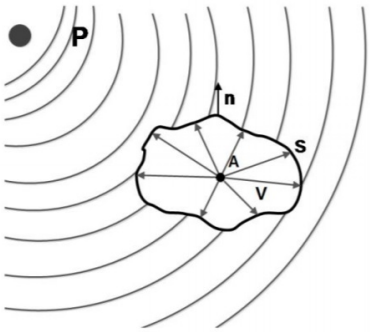

Figure 3.3: Geometry for the Kirchhoff-Helmholtz integral [1]

The Kirchhoff-Helmholtz integral can be expressed as [1] [17],

$$P(\mathbf{R_A}) = -\frac{1}{4\pi}\oint_S [P(R)\nabla G(R, R_A) - G(\mathbf{R}, \mathbf{R_A})\nabla P((R))]\mathbf{n}dS \tag{3.8}$$

where the integral is over $\mathbf{R} = (x, y, z)$ on the surface S.

The acoustic wave field $P(\mathbf{R})$ satisfies in V the two-way wave equation,

$$\nabla^2 P(\mathbf{R}) + k^2(\mathbf{R})P((\mathbf{R}) = 0 \tag{3.9}$$

Likewise, the Green's function $G(\mathbf{R}, \mathbf{R_A})$ satisfies in V the inhomogeneous wave equation with a point source at A,

$$\nabla^2 G(\mathbf{R}, \mathbf{R_A}) + k^2(R)G(\mathbf{R}, \mathbf{R_A}) = -4\pi\delta(\mathbf{R} - \mathbf{R_A}) \tag{3.10}$$

with $\delta(\mathbf{R} - \mathbf{R_A}) = \delta(x - x_1)\mathsf{x}(y - y_1)$ being the product of two Dirac delta functions. Therefore, the Green's function can be explained as the spatial impulse response of the medium in the volume V.

The two dimensional Kirchhoff-Helmholtz equation can be obtained assuming that the wave field $P(\mathbf{r})$ is independent of the y coordinate,

$$P(\mathbf{r_A}) = -\frac{1}{4\pi}\int_C [P(\mathbf{r})\nabla g_2(\mathbf{r}, \mathbf{r_A}) - g_2(\mathbf{r}, \mathbf{r_A})\nabla P(\mathbf{r})]\mathbf{n}dS \tag{3.11}$$

where $\mathbf{r_A} = (x, z)$, the integral is over positions $\mathbf{r} = (x, z)$ on the closed contour C, which encloses the area S_C and $g = (\mathbf{r}, \mathbf{r_A})$ is a two dimensional Green's function.
We can now write the 2-dimensional Helmholtz equation,

$$\nabla^2 P(\mathbf{r}) + k^2(\mathbf{r})P(\mathbf{r}) = 0 \tag{3.12}$$

The two dimensional Green's function $g_2 = (\mathbf{r}, \mathbf{r_A})$ satisfies in S_C the inhomogeneous wave equation with a point source at A,

$$\nabla^2 g_2(\mathbf{r}, \mathbf{r_A}) + k^2 g_2(\mathbf{r}, \mathbf{r_A}) = -4\pi\delta(\mathbf{r} - \mathbf{r_A}) \tag{3.13}$$

The closed contour C consists of the arc C_1 with R radius and the segment C_0 at $x = x_0$. The contribution of the Kirchhoff-Helmholtz integral over C_1 to the pressure in A, vanishes if r goes to infinity.

The Green's function choice is important as it must have a contribution from a source at r_A, in order to satisfy equation 3.13.

Additional contribution from sources outside the contour C can also be added to the Green's function. If these contributions are two monopole sources placed symmetrically with respect to $x = x_0$ in points

$\mathbf{r_A}$ and $\mathbf{r_B}$ its value is,

$$g_2(\mathbf{r}, \mathbf{r_A}) = g(\mathbf{r}, \mathbf{r_A}) - g(\mathbf{r}, \mathbf{r_B}) \tag{3.14}$$

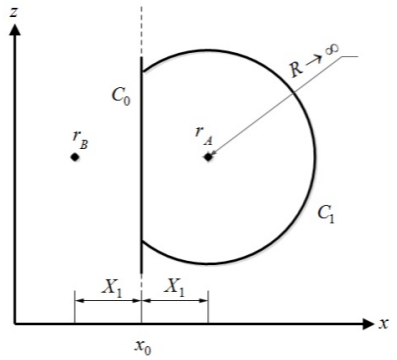

Figure 3.4: Geometry for the Kirchhoff-Helmholtz integral [1]

With the two monopole sources, $g_2 = 0$ on C_0 and the contour C only consists in the line segment C_0. Equation 3.11 results,

$$P(\mathbf{r_A}) = -\frac{1}{4\pi}\int_{-\infty}^{+\infty}(P(\mathbf{r})\nabla g_2(\mathbf{r}, \mathbf{r_A}))_{x=x_0}\mathbf{n}dz \tag{3.15}$$

with $\nabla g_2(\mathbf{r}, \mathbf{r_A})\mathbf{n} = -2\frac{dg}{dx}$, the equation above becomes,

$$P(\mathbf{r_A}) = \frac{1}{2\pi}\int_{-\infty}^{+\infty}(P(\mathbf{r})\frac{dg(\mathbf{r}, \mathbf{r_A})}{dx})_{x=x_0}dz \tag{3.16}$$

This integral is known in acoustics as the Rayleigh II integral [18].

3.2.3 General Green's Function Method

For a system with a ground surface at $z = 0$, equation 3.16 becomes,

$$q(\mathbf{r_A}) = \frac{1}{2\pi}\int_{0}^{+\infty}(q(r)\frac{dg(\mathbf{r}, \mathbf{r_A})}{d\mathbf{r}})_{r=r_0}dz \tag{3.17}$$

where $\mathbf{R_A} = (r_A, z_A)$, **R**=(r,z) and the ground surface is located at $z = 0$.

The Green's function $g(\mathbf{R}, \mathbf{R_A})$ also satisfies the two-dimensional Helmholtz equation and can be written as follows,

$$(\frac{d^2}{dr^2} + \frac{d^2}{dz^2} + k^2(z))g(\mathbf{R}, \mathbf{R_A}) = -4\pi\delta(\mathbf{R} - \mathbf{R_A}) \tag{3.18}$$

Where is assumed that the medium is independent of the horizontal distance, so the range dependence is taken into account by changing k between sequential horizontal steps and g can be written as $\mathbf{g}(\Delta r, z, z_A)$, with $\Delta r = r_A - r$ as the horizontal spacing.

To express the Green's function in terms of the horizontal wave number k_h, the following Fourier transform is introduced,

$$G(k_h, z, z_A) = \int g(\Delta r, z, z_A) e^{-ik_h \Delta r} d(\Delta r) \tag{3.19}$$

The inverse Fourier transform formula,

$$g(\Delta r, z, z_A) = \frac{1}{2\pi} \int G(k_h, z, z_A) e^{ik_h \Delta r} dk_h \tag{3.20}$$

is now substituted in equation 3.19, with $r_A = \Delta r + r$ and $dr = -d_{\Delta r}$. Taking into account Fourier transform properties, equation 3.17 results,

$$q(\Delta r + r, z) = \frac{1}{4i\pi^2} \int_{-\infty}^{+\infty} k_h e^{ik_h \Delta r} dk_h \int_0^{+\infty} G(k_h, z', z) q(r, z') dz' \tag{3.21}$$

The previous expression can also be derived from the spectral theorem of functional analysis [12].

The Green's $G(k_r, z', z)$ function also satisfies the transformed version of the Helmholtz equation and is obtained as follows,

$$\int_{-\infty}^{+\infty} [(\frac{d^2}{dr^2} + \frac{d^2}{dz^2} + k^2(z)) g(r, z; r_A, z_A)] e^{-ik_h \Delta r} d(\Delta r) - 4\pi \int_{-\infty}^{+\infty} \delta(\Delta r) \times \delta(z - z_A) e^{-ik_h \Delta r} d(\Delta r) \tag{3.22}$$

Applying the Fourier transform properties it reduces to,

$$(\frac{d^2}{dz^2} - k_h^2 + k^2(z)) G(k_h, z', z) = -4\pi \delta(z - z') \tag{3.23}$$

3.2.4 Constant Sound Speed Profile

For a non-refracting atmosphere we have a constant wave number, such that $k(z) = k_0$, where k_0 is a reference wave number at the ground surface.

In this situation, for a system with a ground surface at zero height, the solution of equation 3.23 is [19],

$$G(k_h, z', z) = \frac{2\pi i}{k_v} (e^{ik_v |z - z'|} + R(k_v) e^{ik_v |z - z'|}) \tag{3.24}$$

where k_v is the vertical wave number defined by

$$k_v^2 = k^2(z) - k_h^2 \tag{3.25}$$

and is the plane wave reflection coefficient defined as follows,

$$R(k_v) = \frac{k_v Z_g - k_0}{k_v Z_g + k_0} \tag{3.26}$$

where Z_g is the normalized impedance of the ground surface, as explained previously. Substituting equation 3.24 into 3.21 results,

$$q(\Delta r + r, z) = \frac{1}{i\pi} \int_{-\infty}^{+\infty} k_h e^{ik_h \Delta r} dk_h \int_0^{+\infty} \frac{i}{2k_v} (e^{ik_v|z-z'|} + R(k_v) e^{ik_v|z-z'|}) q(r, z') dz' \tag{3.27}$$

A derivation of the governing equation of the GFPE method can be obtained by applying the residue theorem and manipulating the integrals in equation 3.27 in order to get a unique dependence on the wave number [1],

$$\begin{aligned} q(\Delta r + r, z) = \frac{1}{2\pi} \int_{-\infty}^{+\infty} e^{i\Delta r\sqrt{k_0^2 - k_z^2}} e^{ik_z z} dk_z \int_0^{+\infty} e^{-ik_z z'} q(r, z') dz' \\ + \frac{1}{2\pi} \int_{-\infty}^{+\infty} R(K_z) e^{i\Delta r\sqrt{k_0^2 - k_z^2}} e^{ik_z z} dk_z \int_0^{+\infty} e^{ik_z z'} q(r, z') dz' \\ + 2i\beta e^{-i\beta z} e^{i\Delta r\sqrt{k_0^2 - \beta^2}} \int_0^{+\infty} e^{-i\beta z'} q(r, z') dz' \end{aligned} \tag{3.28}$$

Where β is the surface wave pole coefficient which [1] describes with detail by using the residue theorem, the proof for both identities.

$$\beta = \frac{k_0}{Z_g} \tag{3.29}$$

The three terms of the right hand side of the equation 3.28 represents the sum of different types of sound waves. The first term represents the direct wave, the second term represents the wave reflected by the ground and the third term represents the surface wave.

Equation 3.28 is the applied equation for the Green's Function Parabolic Equation method with a non-refracting atmosphere. In the next section, atmospheric refraction is included.

3.2.5 Non-constant speed profile

In the previous section, the equation for the GFPE method with a non-refracting atmosphere was calculated. In this section, an equation for a refractive atmosphere is presented. The variation in each horizontal range step is small enough to assume that the wave number is only a function of height z, therefore its value is,

$$k^2(z) = k_a^2 + \delta k^2(z) \tag{3.30}$$

where k_a is a constant wave number at some average height. Usually it takes the correspondent value at the ground surface $k_a = k(0)$.
The second term on the right-hand side of equation 3.30 is the variation of the vertical profile, which can be either positive or negative and it is always small compared with $k^2(z)$.
Equation 3.7 can be written as,

$$\frac{d^2}{dr}q(r,z) + Qq(r,z) = 0 \tag{3.31}$$

where the operator Q is defined as being independent of range.
Two-way wave propagation is described by,

$$\frac{dq(r,z)}{dr} = \pm i\sqrt{Q}q(r,z) = 0 \tag{3.32}$$

where the positive sign refers to waves travelling to the positive direction of r, and the negative sign applies to waves travelling to the negative direction of r. With the r dependence in q written explicitly and the z dependence implicit, the above equation results,

$$q(r + \Delta r) = e^{i\Delta r\sqrt{Q}}q(r) \tag{3.33}$$

Where for a refracting atmosphere, the operator Q is,

$$Q = d_z^2 + k_a^2 + \delta k^2(z) \tag{3.34}$$

The square root of the operator Q can be approximated as [12],

$$\sqrt{Q} \approx \sqrt{d_z^2 + k_a^2} + \frac{\delta k^2(z)}{2k_a} \tag{3.35}$$

An alternative approximation of the square root operator is described further. Substituting the above equation into the one-way equation 3.33 results,

$$q(r + \Delta r) = e^{i\Delta r\sqrt{d_z^2 + k_a^2 + \frac{\delta k^2(z)}{2k_a}}}q(r) \tag{3.36}$$

assuming that $\sqrt{d_z^2 + k_a^2}$ commutes with $\frac{\delta k^2(z)}{2k_a}$, equation above results,

$$q(r + \Delta r) \approx e^{i\Delta r \frac{\delta k^2(z)}{2k_a}} e^{i\Delta r\sqrt{Q_2}} q(r) \tag{3.37}$$

The above equation is the same as equation 3.33 minus the exponential factor $i\Delta r \frac{\delta k^2(z)}{2K_a}$, thus, is possible to include atmospheric refraction by multiplying the solution in a non-refracting atmosphere by a phase factor, as long as $\delta k^2(z)$ is small relative to $k^2(z)$.

This method of splitting the effect of refraction in two terms, was first used in ocean acoustics and is known as the Fourier split-step algorithm [11].

Replacing $q(r)$ with $\psi(r, z) = e^{-ik_a r} q(r, z)$ for improved accuracy in numerical computations and including the refraction factor $e^{i\Delta r \frac{\delta k^2(z)}{2k_a}}$ equation 3.28 results,

$$\begin{aligned}\psi(r + \Delta r) = e^{i\Delta r \frac{\delta k^2(z)}{2k_a}} \frac{1}{2\pi} \Big(\int_{-\infty}^{+\infty} [\psi(r, k_z) + R_P(K_z)\psi(r, -k_z)] e^{i\Delta r(\sqrt{k_a^2 - k_z^2} - k_a)} e^{izk_z} dk_z \\ + 2i\beta\psi(r, \beta) e^{i\Delta r(\sqrt{k_a^2 - \beta^2} - k_a)} e^{-i\beta z} \Big)\end{aligned} \tag{3.38}$$

where the spatial Fourier transform of $\Psi(r, z)$ is,

$$\Psi(r, k_z) = \int_0^{+\infty} \psi(r, z') e^{iz' k_z} dz' \tag{3.39}$$

Equations 3.38 and 3.39 are the main equations of the GFPE method with atmospheric refraction, which are used in the computational program of this thesis when considering an inhomogeneous atmosphere.

3.3 Extra-Wide-Angle GFPE

Several areas of physics require accurate and robust algorithms for wave propagation at large angles with respect to the nominal direction. Wide-angle propagation occurs in three main cases:

(i) sound waves are reflected from boundaries of a medium

(ii) the sound wavelength is comparable to the scale of medium inhomogeneities, thus resulting in scattering at large angles

(iii) the refractive index of a medium changes significantly in the direction perpendicular to the nominal.

A new approach for Wide-Angle Parabolic Equations was developed by Ostashev which accounts for propagation angles up to 90° with respect to the nominal direction. Since the maximum propagation angle for a WAPE is typically around 40°, this equation is called here an extra-wide-angle parabolic equation (EWAPE) [20].

There are different ranges of applicability of the EWAPEs and WAPEs, being one of them the sound propagation in the atmosphere, done by using the GFPE method.

As indicated above, in the current version of the GFPE, the phase factor due to the refractive index variations is formulated in the narrow-angle approximation. In this section, we provide the GFPE with the wide-angle phase factor.

In a motionless medium, the GFPE with the wide-angle phase factor can be written as follows,

$$p(r,z) = \int_{-\infty}^{\infty} e^{ikz+i\Delta r\sqrt{k_0^2(\epsilon(r_0,z))-k^2}} \times [p(r_0,k) + R(k)p(x_0,-k)]dk \\ +i4\pi k_s p(x_0,k_s) \times e^{-ik_s z+i\Delta r\sqrt{k_0^2(\epsilon(r_0,z)-k_s^2}} \tag{3.40}$$

Where z is the transverse coordinate, R is the plane-wave reflection coefficient, k_s is the complex wavenumber pertinent to a surface wave, $\epsilon(r_0,z)$ is the refractive index and,

$$p(r,k) = \int_{-\infty}^{\infty} e^{-ikz} p(r,z)dz \tag{3.41}$$

The three terms on the right-hand side of the equation above correspond to the direct, ground reflected, and surface waves respectively. If $\epsilon = 0$, sound propagates in a homogeneous atmosphere above an impedance ground and the equation is an exact result.

If $\epsilon = constant$, the equation is still an exact result and can be obtained from writing the reference wave number as $k_0\sqrt{1+\epsilon}$. Equation 3.40 is a new result and it present the GFPE method with the wide-angle phase factor being termed as Extra-Wide-Angle GFPE, or simply EWAPE, and its numerical implementation is similar to the previous equations studied for GFPE.

In appendix B is shown 6 plots where the EWAPE equations were implemented along with the normal GFPE to verify and validate the sound pressure results. It was successfully achieved its validation for an homogeneous atmosphere above a ground impedance depending on the frequency. Were runned several test for $f = 10Hz$, $f = 100Hz$ and $f = 1000Hz$ for a range of $R = 200m$ and $R = 10km$ considering a constant sound speed profile. All the other parameters involved were the same as mentioned in further section 4, in the GFPEs validation subsection, and the benchmark results were taken from reference [9]. Since the elevation angles are very small between the several positions of the source and receiver, this new approach was not used in the further simulations described in chapter 6.

4

Numerical Implementation

The numerical implementation of the Green's Function Parabolic Equation propagation model is based on the computation of equations 3.38 and 3.39. According to their mathematical nature, it is observable that numerical methods are required in order to solve these expressions, which will be described further in this chapter.

As the GFPE method is a step by step extrapolation of the sound field , a two dimensional rectangular grid is used, with two grid parameters (horizontal spacing and vertical spacing) depending on frequency. The length of the numerical grid is defined by the number of horizontal steps necessary to reproduce the horizontal distance between the source and the receiver.

Simultaneously, the grid is limited by the ground surface at $z = 0$ and at a height $z_{TOP} = M\Delta z$, where M is a positive integer and dependent on the source height.

In order to prevent unwanted reflection from sound waves at the truncated top surface, an absorption layer is located between z_{abs} and z_{top}, which will be described further.

4.1 Starting Field

As the GFPE method is a step by step extrapolation, the first step must be to define $\phi(0, z)$ as a starting field function that represents a monopole source.

The complex pressure amplitude in an unbounded non-refracting atmosphere is represented by a harmonic spherical wave and can be written as follows,

$$p(R) = S\frac{e^{ik\mathbf{R}}}{\mathbf{R}} \tag{4.1}$$

where $p(\mathbf{R})$ is the complex pressure amplitude, S is a constant and $\mathbf{R}$ is the radial distance from the source to the receptor.

However this equation cannot be used in the actual algorithms as it diverges at the source when the distance reaches zero and consequently leads to numerical errors.

Therefore is used a Gaussian starting field defined as [1],

$$q(0, z) = e^{\frac{-k_a^2 z^2}{B}}\sqrt{ik_a}(A_0 + A_2 k_a^2 z^2 + A_4 k_a^4 z^4 + A_6 k_a^6 z^6 + A_8 k_a^8 z^8) \tag{4.2}$$

where the coefficients A and B are dependent on the order of the Gaussian field and for convenience are presented on the following table [1]:

For a source near a ground surface, it is mandatory to include the contribution from the reflected wave as

$$q(0, z) = q_0(z - z_s) + \frac{-1 + Z_g}{1 + Z_g}q_0(z + z_s) \tag{4.3}$$

Order	A_0	A_2	A_4	A_6	A_8	B
0	1	0	0	0	0	2
2	1.3717	-0.3701	0	0	0	3
4	1.9705	-1.1685	0.0887	0	0	3
8	9.6982	-20.3785	6.0191	-0.4846	0.0105	3

Figure 4.1: Values of coefficients A and B

Where q_0 is calculated by equation 4.2 and z_s is the source height above the ground surface. In order to allow an accurate comparison with other methods, we use a Gaussian starting field given by [21],

$$\psi(z) = \sqrt{k_a} e^{[\frac{-k_a^2}{2}(z-z_s)^2 + \frac{Z_g - 1}{Z_g + 1} e^{(\frac{-k_a^2}{2}(z+z_s)^2)}]} \tag{4.4}$$

4.2 Fourier Integral's Discretization

The determination of the sound field at each range step requires the computation of several Fourier integrals, as shown previously.As the sound field is being calculated in a numerical grid, by adopting the discrete domain, it can be shown that each of the integrals may be regarded as a sum called Discrete Fourier Transform (DFT).

Following the procedure developed in the literature [22], the Fourier transform in its discrete form is ,

$$\Psi(r, k_n) = \int_0^{+\infty} \psi(r, z') e^{-iz' k_z} dz' \tag{4.5}$$

Where it can be approximated by the following sum

$$\Psi(r, k_n) = \sum_{j=0}^{N-1} (\psi(r, z_j) e^{-ik_n z_j}) \Delta z \tag{4.6}$$

Variable k_z and z' were discretized as,

$$\begin{cases} k_n = n\Delta k, & \text{n=0,1,2,3...N/2,-N/2+1,-N/2+2,...,-1} \\ z_j = j\Delta z, & \text{j=0,1,2,3...N-1} \end{cases} \tag{4.7}$$

where $\Delta k = \frac{2\pi}{N\Delta z}$, Δz is the vertical spacing and $N = 2M$ is the Fourier transform size.

As a consequence of Fourier transform's periodic nature, the vector elements $\Psi(r, k_n)$ and $\Psi(r, -k_n)$ can be related between them by a permutation of vector positions. Thus, it's possible to include both terms into just one transformation.

Following the definition of a DFT [23] the integral $\psi(r, \beta)$ is calculated with a single summation of N

terms as follows,

$$\Psi(r,\beta) \approx (\sum_{j=0}^{N-1} \psi(r,z_j)e^{-i\beta z_j})\Delta z \tag{4.8}$$

After the above integrals have been evaluated, the inverse Fourier integral can be calculated with an analogous approximation,

$$\psi(r,z_j) \approx (\sum_{n=0}^{N-1} \Pi(r,k_n)e^{ik_n z_j})\Delta k \tag{4.9}$$

Where,

$$\Pi(r,k_n) = e^{i\Delta r(\sqrt{k_a^2-k_z^2}-k_a)}[\Psi(r,k_n) + R(K_n)\Psi(r,-k_n)] \tag{4.10}$$

Now it's possible to calculate equation 3.5 by using the above equations,

$$\psi(r+\Delta r,z) = e^{i\Delta r\frac{\delta k^2(z)}{2k_a}}[\frac{1}{2\pi}\psi(r,z_j) + 2i\beta\Psi(r,\beta)e^{-i\beta z_j}e^{i\Delta r(\sqrt{k_a^2-\beta^2}-k_a)}] \tag{4.11}$$

For each one range step is required two Fourier transforms, one forward and one inverse.

An alternative method for computing the Fourier integrals is based on the midpoint rule for numerical integration [24], thus the Fourier integral represented by equation 4.6 results in the following approximation,

$$\Psi(r,k_n) = \sum_{j=0}^{N-1}(\psi(r,z_j+\frac{1}{2}\Delta z)e^{-ik_n z_j})e^{-\frac{1}{2}i\Delta z k_n}\Delta z \tag{4.12}$$

Equation 4.12 uses the coordinates at the center of the integration intervals therefore, the ground surface where $z = 0$ is represented more accurately. This leads to a more precise approximation. The inverse Fourier transform integral results as follows,

$$\varphi(r,z_j) = \sum_{n=0}^{N-1}(\Pi(r,k_n+\frac{1}{2}\Delta k)e^{ik_n z_j})e^{\frac{1}{2}i\Delta k z_j}\Delta k \tag{4.13}$$

4.3 Fast Fourier Transform

The direct calculation of the discrete sums demand a lot of computational effort ant therefore is used an algorithm called Fast Fourier Transform (FFT) to calculate the forward DFT and its inverse. It produces exactly the same results as evaluating the DFT directly although much faster.

The chosen FFT in the computational program was the "Fastest Fourier Transform in the West" [25] written in C language and computes multidimensional complex discrete Fourier transforms of an arbitrary size [26].

4.4 Artificial Absorption Layer

In real outdoor sound propagation, the atmosphere can be considered as an infinite medium regarding its vertical dimension, where sound waves travel until their amplitude reaches zero. However, the discrete formulation of the governing equations requires a finite length of the atmosphere and consequently introduces unwanted and unrealistic reflections of sound waves at the top of the numerical grid.

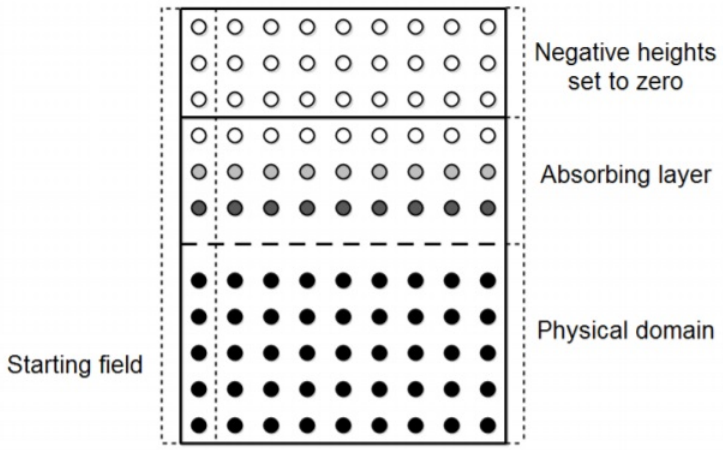

Figure 4.2: Representation of the grid [1]

This numerical error can be eliminated by introducing an artificial absorption layer at the top of the grid which attenuates the sound waves travelling upwards and reaching the maximum height discretized [19]. The implementation of such attenuation layer involves the manipulation of the wave number at the affected grid points by adding an imaginary part to its real value as follows,

$$k_{abs} = k(z) + i\alpha(z) \tag{4.14}$$

Where,

$$\alpha(z) = A(\frac{z - z_{abs}}{z_{top} - z_{abs}})^2 \tag{4.15}$$

and A is a frequency dependent attenuation factor [1] defined further,z_{abs} is the initial height of the absorption layer and z_{top} is the maximum height of the numerical grid.

The absorption layer discussed in this section has a thickness based on the wavelength of travelling sound waves and is typically delimited by 50λ and 100λ to avoid increasing the size of the Fourier transforms used in this propagation method.

By increasing the number of vertical points up to a certain level, it is possible to obtain irrelevant sound wave amplitude values but this method is unpractical since it increases the computational effort.

$f(Hz)$	≤ 16	31.5	63	125	250	500	≥ 1000
$A(m^{-1})$	0.1	0.2	0.3	0.4	0.5	0.5	1

Figure 4.3: Values of A for each frequency interval

Figure 4.4 shows a 2D plot using the simulation parameters from a test case [9] using an absorption layer of 20m thickness. The left plot shows that over 300m of height the absorption layer attenuates all the sound waves and the right plot shows a situation when there is no absorption layer which is equivalent as if the layer thickness was not enough to attenuate the sound waves completely. The right plot above displays the existence of sound waves reflected, as a consequence of the computational method, which creates interferences [4]. Therefore, to ensure more precise results the absorption layer is used in all simulations.

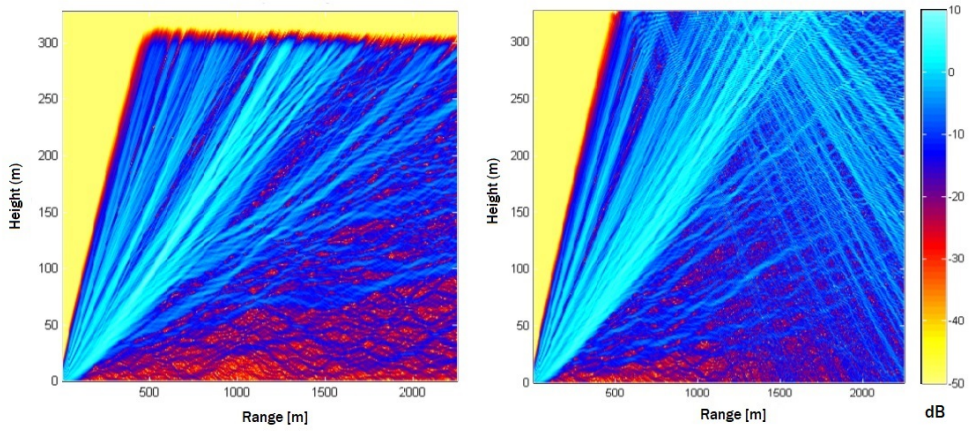

Figure 4.4: 2D Plots of sound waves amplitude with absorption layer (Left) and without absorption layer (Right)

4.5 Window Function

The discrete sampling of the inverse Fourier transform causes errors when its summand oscillates rapidly. It is given by the following equation,

$$S(k_n) = \frac{1}{N\Delta z}(\Psi(r,k_n) + R_P(K_n)\Psi(r,-k_n)]e^{i\Delta r(\sqrt{k_a^2-k_z^2}-k_a)}e^{izk_n}) \tag{4.16}$$

Therefore, the summand is multiplied by the window function to suppress its rapid oscillation [1],

$$\begin{cases} 1, & |k| < 0.5k_a \\ cos^2(\frac{\pi(|k|-0.5k_a)}{k_a}), & 0.5k_a \leq |k| \leq k_a \\ 0, & |k| > k_a \end{cases} \tag{4.17}$$

The window function acts like a numerical filter in k domain, suppressing the errors caused by the discrete sampling of the inverse Fourier Transform given by,

$$C(k_n) = \sum_{i=0}^{n} S(k_i) \tag{4.18}$$

4.6 Alternate Refraction Factor

In the Green's Function Parabolic Equation method, atmospheric refraction was taken into account by multiplying the solution by a exponential factor given by,

$$e^{i\Delta r \frac{\delta k^2(z)}{2K_a}} \tag{4.19}$$

An alternate exponential factor that provides more accurate results than the one defined was developed further. The derivation of this refraction factor is based on the expansion of the square-root operator $\sqrt{Q}$ [27] and can be defined as [1],

$$e^{i\Delta r \delta k^2(z)} \tag{4.20}$$

4.7 GFPE's Validation

Several tests were made to analyze the accuracy of the GFPE method described. Three test cases were used where the sound speed profiles for each test case are given in figure down,

Test Case	1	2	3
Sound speed profiles	Homogeneous	Downward	Upward
Speed c (m/s)	$c = 343$	$c = 343 + z/10$	$c = 343 - z/10$

Figure 4.5: Sound speed profiles for each test case

For the simulations a range of R=200m and R=2000m was considered [1],

In these test cases the ground is assumed to be transversely uniform, to have range independent properties and to be a completely flat ground surface. The ground impedance represent grassland. These ground impedance values are obtained with the following equations,

$$Z_g = \frac{w\rho_b}{k_b \rho_0 c_0} \tag{4.21}$$

Ground Surface	Absorbing
$10\ Hz$	$Z_g = 38.79 + 38.41i$
$100\ Hz$	$Z_g = 12.81 + 11.62i$
$1000\ Hz$	$Z_g = 5.96 + 2.46i$
Source Height (m)	5
Receiver Height (m)	1

Figure 4.6: Ground parameters for the test cases

Where,

$$\begin{cases} k_b^2 = (\frac{qw}{c_0})^2[1 - 2(\lambda\sqrt{i})^{-1}T(\lambda\sqrt{i})^{-1}(1 + 2(\gamma - 1) \times (N_{Pr}^{\frac{1}{2}}\lambda\sqrt{i})^{-1}T(N_{Pr}^{\frac{1}{2}}\lambda\sqrt{i})] \\ \rho_b = \frac{q^2}{\Omega}\rho_0[1 - 2(\lambda\sqrt{i})^{-1}T(\lambda\sqrt{i})]^{-1} \\ q^2 = \Omega^{-g} \\ \lambda = \frac{1}{2s_f}[\frac{8\rho_0 q^2 w}{\Omega\sigma}]^{\frac{1}{2}} \\ T(x) = \frac{J_1(x)}{J_0(x)} \\ w = 2\pi f \end{cases} \tag{4.22}$$

The parameters are given by the following tabulated values taken from benchmark problems used to test outdoor sound propagation models [9]:

-Porosity Ω = 0.27

-Flow Resistivity σ = 366 $\frac{kPa.s}{m^2}$

-Pore Shape Factor Ratio s_f = 0.75

-Grain Shape Factor g = 0.5

-Air Density $\rho_0(20°)$ = 1.205 $\frac{kg}{m^3}$

-Prandtl Number N_{Pr} = 0.724

-Ratio of Specific Heats γ = 1.4

-Speed of Sound $c_0(20°)$ = 343.23 $\frac{m}{s}$

These test cases have an exact analytical solution, which is useful and fundamental to test the accuracy of the program. The number of vertical points used was 2048 for $10Hz$ and $100Hz$ and 4096 for $1000Hz$.

The values of each grid parameter used in the several case studies adopted in this thesis that fulfill the requirements demanded by each propagation method are described in the next figure [28].

dr	λ
dz	$\lambda/20$
$z_{abs}\ (m)$	300
$z_{top} - z_{abs}$	80λ

Figure 4.7: Numerical parameters for the three test cases

The pressure fields obtained with the GFPE method for the referred specified conditions are displayed in the appendix A.

The results correspond to a homogeneous atmosphere above a flat ground surface and it's possible to conclude that the geometrical spreading is the most influencing parameter in the solution, especially for short distances. As the wave frequency increases the effects of atmospheric absorption become more noticeable for long range propagation, as the shadow region, here represented by the lower limit of the vertical axis, occurs for decreasing ranges with increasing frequencies [13].

For higher distances we may expect that interaction between the surface and the sound waves starts to occur as the multiple sound rays are directed towards the ground and that this phenomenon consequently becomes more significant in the transmission loss evolution. The effects of ground reflections of sound waves may be observed in the graphics on the right side where it's possible to verify that for increasing frequencies the ground interaction is noticeable for decreasing ranges and it appears as non periodic fluctuations in the value of the transmission loss.

From the analysis of the results from case 1 and case 2, we can detect that for short range propagation the speed gradient does not affect the evolution of the transmission loss and therefore the conclusions from test case 1 are also applied to the situation of sound propagation at small distances in a downward refracting atmosphere.

For an upward refracting atmosphere where the sound rays are deflected away from the ground surface towards the top of the atmosphere it's expected the occurrence of a shadow region particularly in long range propagation. The effects of upward refraction are visible for a wave frequency of 1000Hz where an increase in attenuation of about 5dB at a range of 200m when compared with the corresponding results in the previous two test cases.

The influence of upward refraction becomes more important as the shadow region occurs for shorter ranges when compared with the data related to sound propagation in a homogeneous atmosphere. In the first tested simulation the shadow region becomes noticeable at a range of approximately 1600m and 1200m for wave frequencies of 100Hz and 1000Hz respectively, while in test case 3 the shadow region for the same frequencies occurs at 450m and 350m [13].

5

ECAC Trajectory Model

5.1 ANP Database

To make an accurate noise assessment was developed a noise model which allows to make simulations for different aircraft, being chosen Airbus A320-211 for the scope of this thesis. For this effect it was used the ANP database which is an international online data resource accompanied by the ECAC Doc.29 [5] guidance documents on airport noise contour modelling. These documents are the most commonly used database for noise modeling and it contains aircraft and engine performance coefficients for a wide range of commercial aircraft supplied by the manufacturers.

Relationships between the noise levels and slant distances for different engines and power settings can be found on that database through Noise-Power-Distance tables and curves defined for reference conditions, such as steady flight at a reference speed in specified reference conditions and in a specified flight configuration.

It's important to mention that there is no practicable way in which the accuracy of the data entries can be systematically and independently checked, and some inconsistencies are most likely to be found when comparing model predictions with measured data. Nevertheless, the database is subject to constant updates, approved by the suppliers and database managers to keep it as accurate as possible.

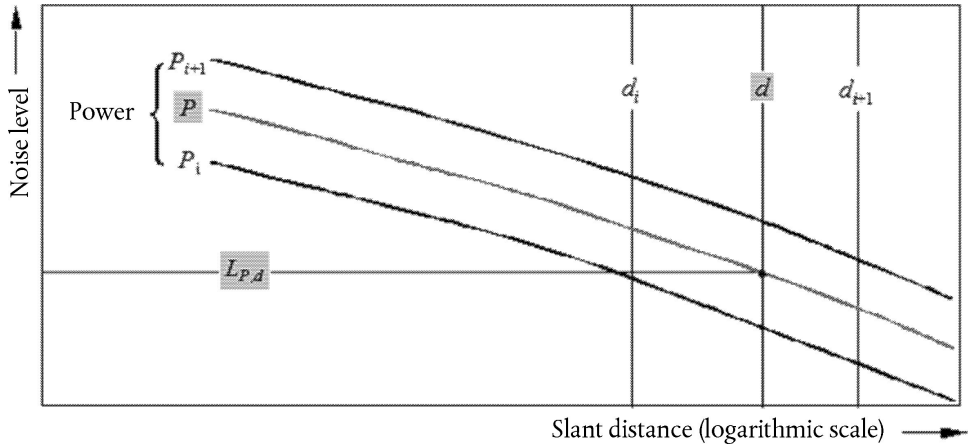

Figure 5.1: Noise-Power-Distance Curves [5]

5.2 Noise Model

ECAC Doc.29 established a combination of logic and mathematics to obtain a physical model capable of calculating noise levels due to aircraft operations in any point.

Typically, modelling systems comprise three main elements, starting by an input of airport and aircraft data such as the runway heading and altitude and weather conditions, the aircraft's engines' and flaps'

coefficients and a set of procedural steps to be modelled.This is followed by the application of the model, which processes the given input and converts it into an accurate and detailed flight path, which is then used to calculate the noise levels at the observer due to that flight departure.

A briefly description of the steps in this process are the following:

1. Pre-Processing of Airport Data
2. Definition of Flight Path
3. Noise level at the observer

5.3 Coordinate System

Before forming any flight path, it wass necessary to define the coordinate systems to be used. With this in mind it was chosen a fixed local coordinate system with its origin at the Montijo's aerodrome as shown in figure 5.2.

Figure 5.2: Montijo Aerodrome's coordinate system used - adapted from GoogleMaps

Figure 5.3: Montijo Aerodrome's runway distance - adapted from GoogleMaps

It was also necessary a 1 dimensional coordinate system which follows the ground track,where its axis is the ground track distance s and has its center on the start of roll in the runway in use. This will be the main system used while modelling the flight paths as it's specific for each ground track, representing a distance s measured along the track throughout the flight direction. In this system, any flight operation parameter is function of the distance s.

For the scope of this thesis, all the distances refered to Montijo's Aerodrome were measured through Google Maps Tools as is seen in figure 5.3.

Finally, a third and last reference system fixed to the aircraft will be used in situations where it's important to know the aircraft's position. This aircraft coordinate system has its origin at the actual

aircraft location, with its x axis following the aircraft's longitudinal axis, y axis following the lateral axis and z following its vertical axis, as shown in the next figure.

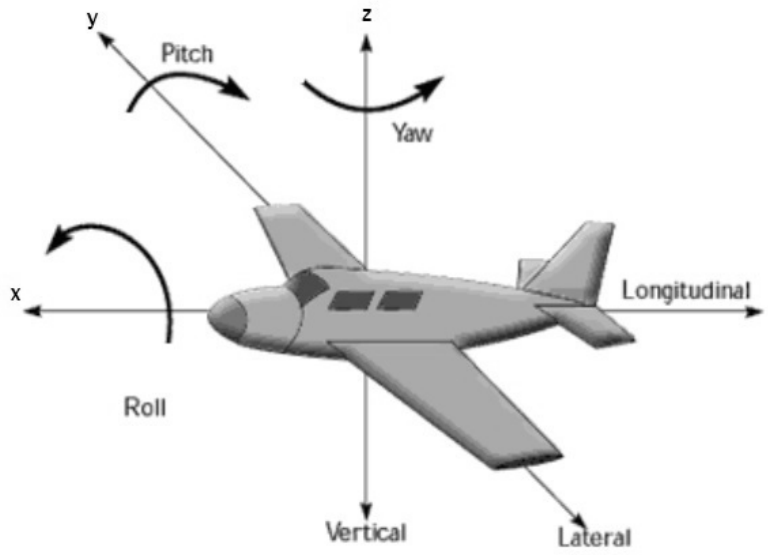

Figure 5.4: Aircraft's fixed coordinate system - adapted from Google images

5.4 Flight Path Segmentation

ACFT_ID	Profile ID	Step	Step Type	Thrust Rating	Flap_ID	End Point Altitude (ft)	Rate Of Climb (ft/min)	End Point CAS (kt)
A320-211	ICAO_A	1	Takeoff	MaxTakeoff	1+F			
A320-211	ICAO_A	2	Climb	MaxTakeoff	1+F	1500.0		
A320-211	ICAO_A	3	Climb	MaxClimb	1+F	3000.0		
A320-211	ICAO_A	4	Accelerate	MaxClimb	1+F		812.1	186.1
A320-211	ICAO_A	5	Accelerate	MaxClimb	1		933.5	201.2
A320-211	ICAO_A	6	Accelerate	MaxClimb	ZERO		1119.7	228.2
A320-211	ICAO_A	7	Accelerate	MaxClimb	ZERO		1240.5	250.0
A320-211	ICAO_A	8	Climb	MaxClimb	ZERO	5500.0		
A320-211	ICAO_A	9	Climb	MaxClimb	ZERO	7500.0		
A320-211	ICAO_A	10	Climb	MaxClimb	ZERO	10000.0		

Figure 5.5: Departure Standard Procedure for Airbus A320-211 [ANP Database]

The segmentation process for the different operations that can be combined to produce a flight path will be detailed throughout this section, including the equations to calculate the flight profile, the required

propulsion to follow the operation and the resulting airspeed as well as all the necessary preliminary data from the ANP database.

Standard procedures have been developed for each aircraft and are also present on the ANP database, as represented previously, in respect to Airbus A320-211.

5.4.1 Aircraft Trajectory

The modeling approach presented in this thesis evaluates procedures to define a small set of trajectory model parameters. The model parameters are grouped according to typical phases of flight.

It is in the scope of this thesis to calculate the trajectory of an aircraft departure, in which are included the following stages of a flight:

1. Take-off Roll
2. Take Off
3. Initial Climb

It was assumed changes of flight parameters between flight-phase events and all aircraft accelerations and decelerations were executed at a constant rate. Most flight phases defined here involve one speed transition where a new target airspeed is established at the beginning of a phase and maintained throughout the remainder of a phase.

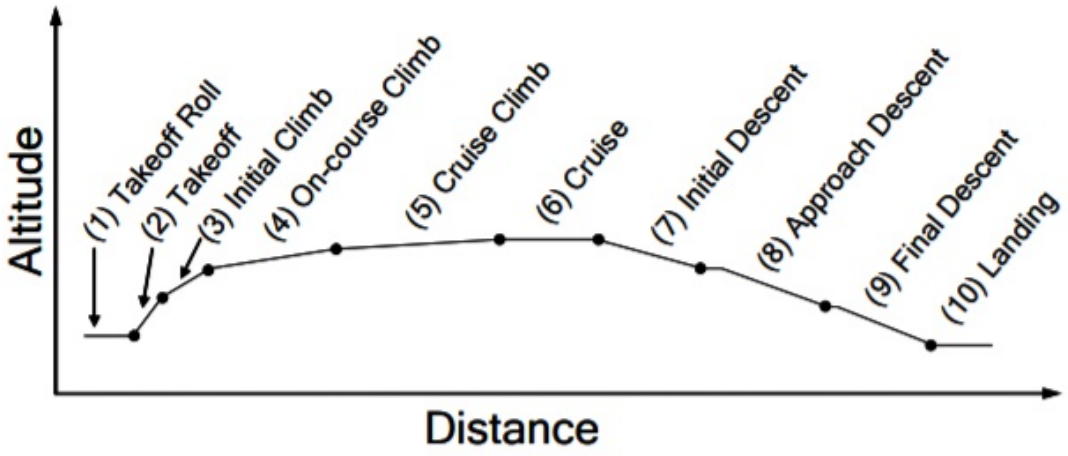

Figure 5.6: Altitude Profile for a Flight Trajectory [6]

For convenience, it will be described briefly the specific flight trajectory stages in the scope of this thesis.

5.4.1.A Takeoff Roll

The objective of the takeoff roll phase of an aircraft is to accelerate sufficiently such that the wings generate adequate lift to safely support the weight of the aircraft when it becomes airborne. The speed at which the aircraft can become airborne is called rotation speed. The beginning of this phase generally coincides with the pilot's application of engine takeoff power.

The resulting forward thrust and acceleration of the aircraft is maintained until rotation speed is achieved which defines the end of the takeoff roll flight phase of the model. Rotation is the process of changing the orientation in space, called attitude, of the aircraft's longitudinal axis from a level attitude to a nose-high takeoff attitude. The parameters that are chosen to describe this phase are the aircraft's takeoff roll acceleration and rotation speed [29].

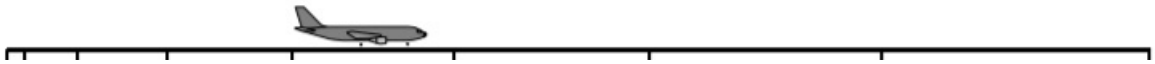

Figure 5.7: Takeoff roll representation [6]

5.4.1.B Takeoff

As the pilot establishes aircraft takeoff attitude during rotation, the lift produced by the wings increases and supports the weight of the aircraft. The resulting increase in aerodynamic drag leads to a significantly reduced takeoff acceleration. When the aircraft is airborne and a positive climb gradient has been established, the landing gear is raised.

After acceleration to initial climb airspeed, the subsequent climb generally assures obstacle clearance by providing efficient gain in altitude for the distance flown by the aircraft. The takeoff flight phase of the model is concluded when the aircraft has climbed sufficiently and reached a "safe" altitude above ground level where obstacle clearance considerations are no longer a factor. The takeoff phase consists of two parts. The first part is characterized by the aircraft's acceleration to initial climb airspeed and the second part describes a climb at constant indicated airspeed.

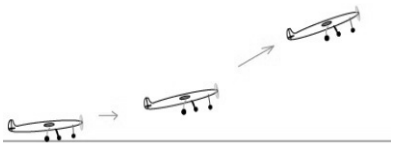

Figure 5.8: Takeoff illustration adapted from Google images

5.4.1.C Initial Climb

When obstacle clearance considerations are no longer a concern, engine power is generally reduced from takeoff thrust to climb thrust in order to minimize the time the engines are subjected to the increased stresses of takeoff power settings. The model maintains initial climb airspeed throughout the initial climb phase.

Maintaining initial climb airspeed while engine power is reduced to climb thrust typically requires a reduction in the flight path's climb gradient. The initial climb flight phase in the model is completed when the aircraft climbs through a target altitude typically measured above ground level. The initial climb gradient and target altitude are the only parameters used to model the initial climb flight phase.

5.5 Flight Profile Segmentation

The parameters describing each flight profile segment at the start and end of the segment are:

- s_1, s_2 distance along the runway
- z_1, z_2 aircraft altitude
- V_1, V_2 aircraft groundspeed
- P_1, P_2 power parameter
- ζ_1, ζ_2 bank angle

To build a flight profile from a set of procedural steps (flight path synthesis), segments are constructed in sequence to achieve required conditions at the end points [29]. The end-point parameters for each segment become the start-point parameters for the next segment.

In any segment calculation the parameters are known at the start; required conditions at the end are specified by the procedural step and the steps themselves are defined by the ANP database. The end conditions are usually height and speed and the profile building task is to determine the track distance covered in reaching those conditions.

If the ground track is straight, the profile points and associated flight parameters can be determined independently of the ground track and therefore the bank angle is always zero, which is the present case on this thesis. If the effects of turns on the flight profile are to be disregarded, in case of straight flight, single segment solution is adopted. 3-D flight path is then generated by merging its 2-D flight profile with its 2-D ground track.

The result is a sequence of co-ordinate sets (x, y, z), each being either a node of the segmented ground track, a node of the flight profile or both, the profile points being accompanied by the corresponding values of height z, ground speed V, bank angle ζ and engine power P. For a track point (x, y)

which lies between the end points of a flight profile segment, the flight parameters are interpolated as follows:

$$z = z_1 + f(z_2 - z_1) \tag{5.1}$$

$$V = \sqrt{V_1^2 + f(V_2^2 - V_1^2)} \tag{5.2}$$

$$P = \sqrt{P_1^2 + f(P_2^2 - P_1^2)} \tag{5.3}$$

$$f = \frac{s - s_1}{s_2 - s_1} \tag{5.4}$$

5.5.1 Takeoff Ground Roll

When taking off, as an aircraft accelerates between the point of brake release (alternatively termed Start-of-Roll SOR) and the point of lift-off, speed changes dramatically over a distance of 1500 to 2500 m, from zero to between around $100m/s$ [29]. The takeoff roll is thus divided into segments with variable lengths over each of which the aircraft speed changes by specific increment ΔV of no more than 10 m/s.

Although it actually varies during the takeoff roll, an assumption of constant acceleration is adequate for this purpose. For equivalent takeoff distance s_{TO} and takeoff speed V_{TO}, the number n_{TO} of segments for the ground roll is given by the following expression:

$$n_{TO} = int(1 + \frac{V_{TO}}{10}) \tag{5.5}$$

Where the change of velocity is given by,

$$\Delta V = \frac{V_{TO}}{n_{TO}} \tag{5.6}$$

Hence, the length $s_{TO,k}$ of each segment k $(1 \leq k \leq n_{TO})$ of the takeoff roll is given by,

$$s_{TO,k} = \frac{(2k-1)s_{TO}}{n_{TO}^2} \tag{5.7}$$

The above equations assume that the initial speed of the aircraft at the start of the takeoff phase is zero which corresponds to the common situation where the aircraft starts to roll and accelerate from the brake release point.

5.5.2 Initial Climb

Right after takeoff, the aircraft climbs with a constant airspeed until a set altitude. From the moment an aircraft leaves the ground, the properties of its noise propagation to the ground vary from point to point.

A single segment for the climb section was shown to provide poor results in terms of noise accuracy. As such, it is recommended to divide it into segments, with the length of each being influenced by lateral attenuation. This results in this section being segmented based on a set of height values given by the following figure [29],

$$z' = \{18.9,\ 41.5,\ 68.3,\ 102.1,\ 147.5,\ 214.9,\ 334.9,\ 609.6,\ 1289.6\}\ metres$$

Figure 5.9: Set of height values

Based on this set of heights, it should be identified which of them is closest upper bound to the section endpoint height, and then calculate each segment's height using:

$$z_{seg_i} = z' \frac{z_i}{z_N}, (i = 1, ..., N) \tag{5.8}$$

Where z_{seg_i} is the height of the i^{th} segment of the climb section, z_i is the i^{th} member of the set of height values, z' is the section endpoint height and z_N is the closest upper bound to height z.

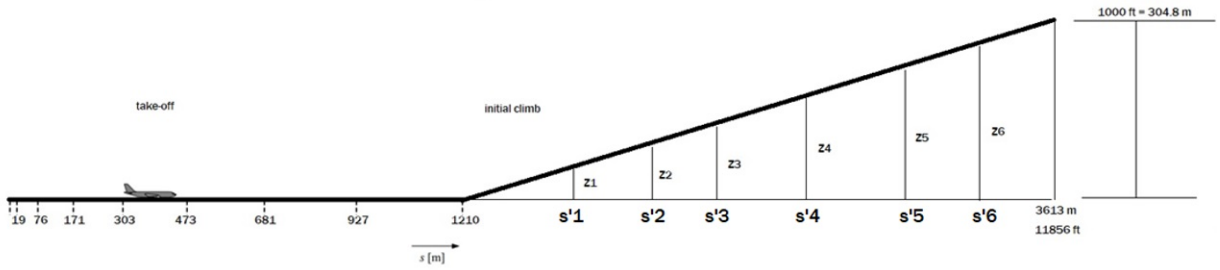

Figure 5.10: Illustration of takeoff roll and initial climb

5.6 Ground Track Segmentation

Designing a ground track is typically a simple process as it consists in a series of lines that are either straight - defined by length Δs and heading ξ, or circular arcs - defined by change of heading $\Delta\xi$ and curve radius R as shown below [29].

With the purpose of making the transition as seamless as possible without turning the curve into a computational burden, any curve is divided into sub-arcs, with the first and last sub-arc functioning as a transition arc. These transition sub-arcs are dictated by the bank angle and change of heading, and are not strictly defined in Doc.29's model. It was assumed for simplicity purposes that the transition change

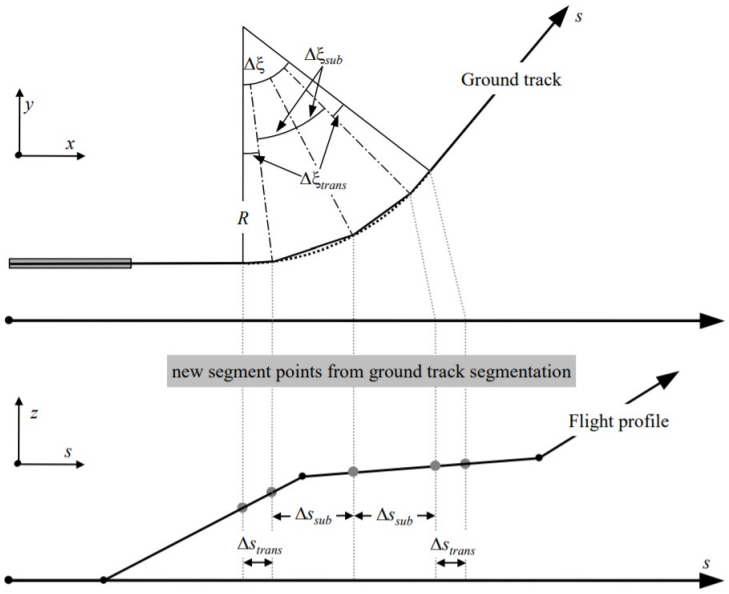

Figure 5.11: Ground track geometry segmentation [5]

of heading is constant and equal to $\Delta\zeta_{trans} = 5$ for every turn. The arc is then divided into n_{sub} sub-arcs according to the following equation:

$$n_{sub} = floor(1 + \frac{\Delta\zeta - 2\Delta\zeta_{trans}}{30}) \tag{5.9}$$

In which floor is a function that rounds the input to the nearest smaller integer number.
The change of heading of each sub-arc $\Delta\zeta_{sub}$ is given by the following expression:

$$\Delta\zeta_{sub} = \frac{\Delta\zeta - 2\Delta\zeta_{trans}}{n_{sub}} \tag{5.10}$$

Where n_{sub} has to be large enough so that $\Delta\zeta_{sub} \leq 30$.

For an aircraft to make a turn and change its heading, it has to change its bank angle ζ by tilting itself towards the side it wants to turns. With this in mind, for an aircraft to make a seamless transition from straight flight to a steady turn, it would need an instantaneous change of bank angle which is not physically possible.

This instantaneous change can be ignored and approximated by assuming a linear increase from its initial value at the beginning of the turn to its final value at a certain distance within the curve, which will be defined as the end of the transitioning sub-arc. This assumption is also followed for the end of the turn, in which the bank angle decreases linearly from the beginning of the transition sub-arc until the end of the turn.

$$\zeta = tan^{-1}(\frac{2.85V^2}{rG}) \tag{5.11}$$

Where V is the groundspeed in knots, r is the radius of the turn in feets and G is the acceleration due to gravity in feets per second squared.

5.7 Noise Calculation

After having trajectory defined by a sequence of points and the mentioned parameters at each of them, it is possible to start calculating noise levels received in different locations relatively to a single aircraft.

The most common metrics used in modern aircraft noise indices are single-event sound exposure levels L_E which take into account all the sound energy in the events, and its exact values are given by the following equation,

$$L_E = 10\log(\frac{1}{t_0}\int_{t_1}^{t_2} 10^{\frac{L(t)}{10}}dt) \tag{5.12}$$

Where t_0 corresponds to a reference time value, $L(t)$ is a noise level curve in function of time and $[t_1, t_2]$ is the time interval which should be chosen in such way that ensures that all the sound resulting from the event is comprised.

It is also used the metric L_{max} that is the maximum instantaneous level in the event.These two metrics will be calculated in this model in a different scale of noise, using the A-weighted filter to represent the human ear's sensitivity to different frequencies, resulting in the metrics L_{Amax} and L_{AE}. This last one can be obtained through the following expression,

$$L_{AE} = 10\log(\frac{1}{t_0}\int_{t_1}^{t_2} 10^{\frac{L_A(t)}{10}}dt) \tag{5.13}$$

with $t_0 = 1$ second and $[t_1, t_2]$ is the time interval where $L(t)$ is 10 dB below L_{max}.

5.7.1 NPD Datasheet

ANP datasheet supplies the necessary data to calculate noise levels at each segment of the flight path. It is possible to obtain values for L_{max} and L_E as functions of propagation distance and also to obtain noise-related power parameter $P = \frac{F_n}{\delta}$ for a specific aircraft.

As this values refer to certain conditions such as the airspeed, and due to the fact that it is under the assumption of infinite flight path instead of small segments, its strictly necessary to correct and adjust all the obtained data as the values in this tables are baseline levels depending on the the power P and distance d, being L_{max} and $L_{E\infty}$.

Due to the fact that this values are tabulated for specific values of (P, d) it's necessary to estimate the noise levels by interpolation and also taking into account the fact that the power parameter for which the noise levels are tabulated varies linearly, and the propagating distance varies logarithmically, a linear

interpolation is used between tabulated power settings and a logarithmic interpolation is used between distances.

The interpolations refered, follow the next equations expressed above,

$$L(P) = L(P_i) + \frac{L(P_{i+1}) - L(P_i)}{P_{i+1} - P_i}(P - P_i) \tag{5.14}$$

$$L(d) = L(d_i) + \frac{L(d_{i+1}) - L(d_i)}{log(d_{i+1}) - log(d_i)}(log(d) - log(d_i)) \tag{5.15}$$

The adjustments to be made to the baseline values obtained from these tables usually take into account as well other effects such as duration corrections, installation effects, lateral attenuation segment correction. For the sake of simplicity, it was only accounted the segment correction which takes into account the finite length of the segments. It is assumed in this model that the aircraft is flying in a straight and steady level flight along an infinite path.

This last correction adjusts the level so that the values are respective to the finite segment only, which obviously contributes less noise exposure than an infinite one, and it's given by the following equation,

$$\Delta_F = 10log_{10}(F) \tag{5.16}$$

Where F is the energy fraction which accounts for the pronounced longitudinal directivity of aircraft noise and is influenced by the slant distance for each segment.

After calculating the values of the correction parameters, the noise levels for each segment can be obtained by the following equations,

$$L_{max,seg} = L_{max}(P, d) \tag{5.17}$$

$$L_{E,seg} = L_{E\infty}(P, d) + \Delta_F \tag{5.18}$$

Having found the values for each segment it is then possible to obtain the the maximum event level L_{max} which is given by the maximum value of $L_{max,seg}$ amongst all segments and the sound exposure level L_E is given by the decibel sum of the contributions of each segment's sound exposure level $L_{E,seg}$. These can be expressed through this next two equations,

$$L_{max} = max(L_{max,seg}) \tag{5.19}$$

$$L_E = 10log(\sum 10^{\frac{L_{E,seg}}{10}}) \tag{5.20}$$

When calculating the sound exposure level in each segment, the distance parameter is different and is referred to as the minimum slant range d_p, which is given by the perpendicular distance from the observer to the infinite-length segment, while on the other hand, when calculating the maximum level metrics, the NPD distance is the shortest distance d_s between the observer and the finite-length segment.

Considering a fixed observer at EXPO (Parque das Nações), the observer will always be ahead of the segment of the flight path and therefore can be represented by the following geometry above [29],

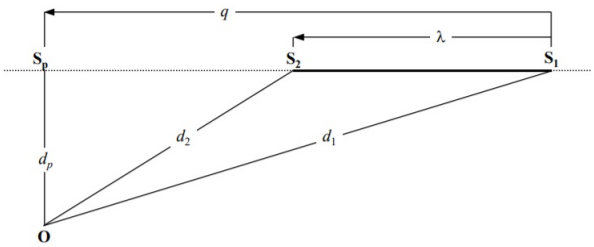

Figure 5.12: Flight path segment geometry for an observer ahead of segment

For claryfing purposes, the next figure presents the location of the fixed observer at zero height AMSL.

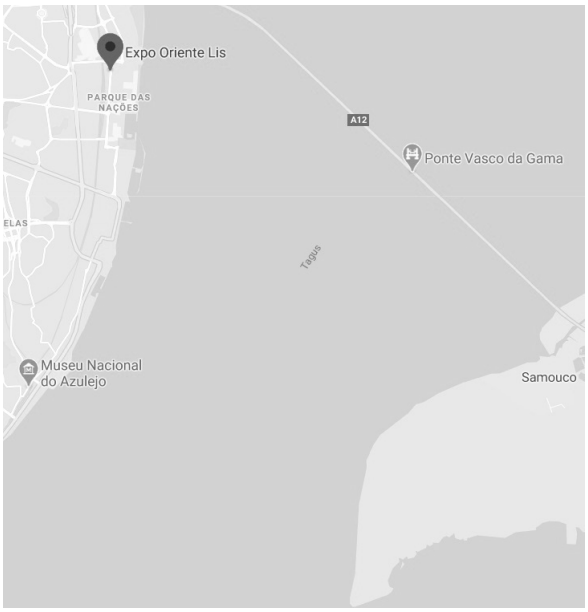

Figure 5.13: Schematic figure of a fixed observer location - adapted from Google Maps

6

Simulations Results

The simulations presented in this section refer to feasible aircraft departure flight trajectories for the Montijo's future airport. Commercial aviation airlines are required to follow standard authorized trajectories for each airport as flight operations are driven under Instrument Flight Rules (IFR), therefore national air traffic management organizations publish and update the departing and arrival procedures, denominated respectively by Standard Instrument Departure (SID) and Standard Terminal Arrival Route (STAR).

Typically, SID procedures are related to the lateral navigation of the airplane and do not include impositions on the climb gradient of the airplane, unless necessary for obstacle clearance or for traffic reasons while in the other hand, STARs establish not only the lateral navigation profile of the approach but also define the approach's vertical profile [30].

In the scope of this thesis was used a NAV-Portugal's study [7] where it was evaluated the viability of arriving and departure routes for the tracks 01 and 19 that mitigate the overflight on the Ponta da Erva zone since it is protected as Natural Reserve. One of the main goals of this study was to evaluate the flight paths along with the maximum climb gradients that would allow to reduce the noise levels. Along the construction of the departure trajectories it was considered the maximum climb gradient with a value of 10%.

6.1 Montijo's Airbase

The airport in study is the Montijo Air Base No.6 (ICAO: LPMT) which is currently a Portuguese Air Force's military air base located at Montijo, near Tejo river with the purpose for maritime patrol, anti-submarine warfare and also for search and rescue operations, being in use since 1953 [31].

This air base consists of two intersecting runways:

1 - Runway 1/19 with 2,147 m length and an asphalt surface;

2 - Runway 08/26 with 2,440 m and a surface in concrete.

Its ARP coordinates are (38° 42' 13.90" N, 009° 02' 09.30" W), and it has a 14 m elevation above mean sea level [32].

The plan to use this air base as an auxiliary aerodrome to Lisbon's main airport assumes the use of runway 01/19 as the main one, being roughly parallel to Humberto Delgado's runway 03/21, the most frequently used one in the airport.

Not only is the use of RWY01-19 convenient based on the fact that Portugal has predominantly Northern winds, but also the usage of runway 08/26 would be incompatible with aircraft approaching or taking off from Humberto Delgado's runway 21 due to possible interference. Furthermore, the installation of an Instrument Landing System (ILS) in runways 01/19 is intended for increased safety, and the creation of a parking platform for aircraft from the different airlines, along with a civil terminal is being considered.

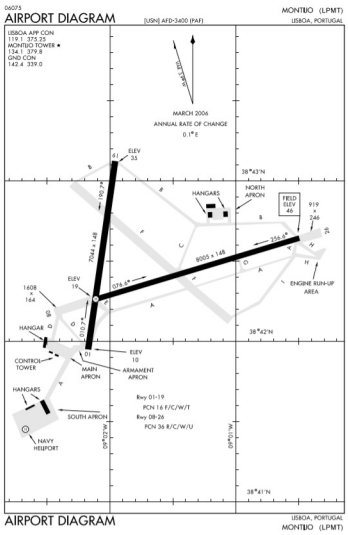

Figure 6.1: Montijo Air Base diagram [7]

Apart from the previously mentioned rules, there are also airspace restrictions and warnings, such as areas with military activities with potential risk to General Air Traffic. Three main categories can be differentiated [33] [34]:

1 - Danger areas, within which dangerous activity may occur at specified times mostly operated by military authorities, making it unsafe for civil aircraft to fly over the area;

2 - Restricted areas, in which the flight of aircraft is restricted in accordance to specific conditions;

3 - Prohibited areas, within which the flight of aircraft is strictly prohibited.

All these areas limits are available in national Aviation Information Publications (AIP) along with the hours of operation where applicable.

It is frequent for many danger and restricted areas to be inactive for long periods of time, which makes the airspace become inefficient as it's not being used for military nor civil purposes. As such, the concept of Flexible Use of Airspace (FUA) has been developed to optimize the use of airspace within Europe. Therefore the airspace is shared through enhanced civil and military co-ordination that ensures that the airspace segregation is temporary and based on real use for specified time periods [35].

For the sake of simplicity and within the scope of this thesis, it will be assumed that the Montijo's Air Base will no longer be used for military purposes only, allowing for civil navigation with no restrictions for any flightpath.

6.2 Departure Flight Path

In order to provide and calculate the instant distances from the aircraft to the fixed observer located at EXPO, it was developed a Matlab script that followed the algorithms explained in section 5.

The script reads the information from the CSV datasheets from ANP Database refering to Airbus A320-211 with motors CFM565 and reads the parameters to execute the flight path segmentation. All the trajectories follow the procedural departure steps from ECAC [29] and simultaneously the flight path sugested by the NAV study.

Figure 6.2: Departure proposal for track 01 with 10% climb gradient [7]

Based in the plotted figure it is understood that the flight path is constituted by a straight line until the PISCO zone, then a turn with with circular geometry and then another straight line until the DANIL zone. It was considered three different departure flight paths in which only vary the turning radius after the PISCO zone. It was adopted a turning radius of 5.000ft (test case 1), 10.000ft (test case 2) and 20.000ft (test case 3). For all of them the climbing rate was constant.

The referred Matlab script generates a text file with the several coordinates (x, y, z) of the aircraft for the coordinate system framed in Montijo's groundtrack and also the absolute distance from the aircraft to the observer.

The several trajectory plots for each test case are displayed above with the PISCO and DANIL zones marked.

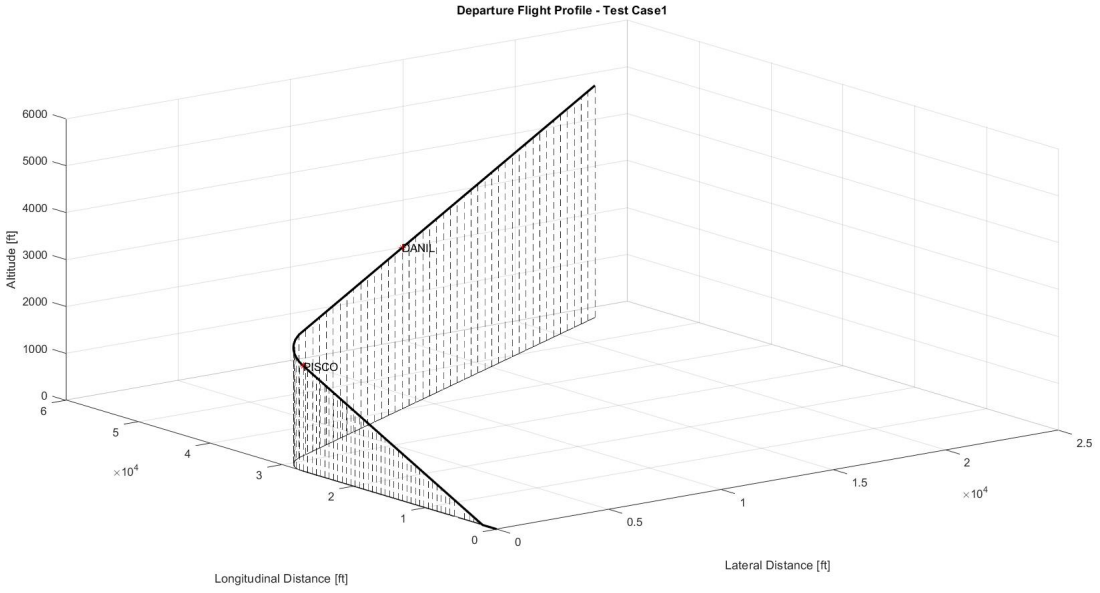

Figure 6.3: Flight path - Test case 1 with turning radius of 5.000ft

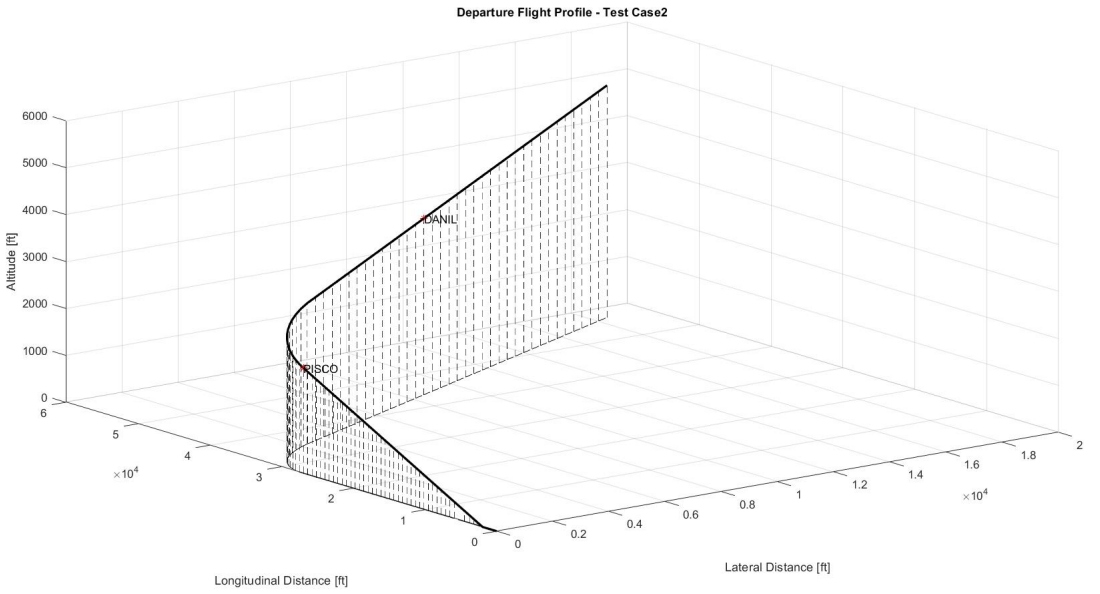

Figure 6.4: Flight path - Test case 1 with turning radius of 10.000ft

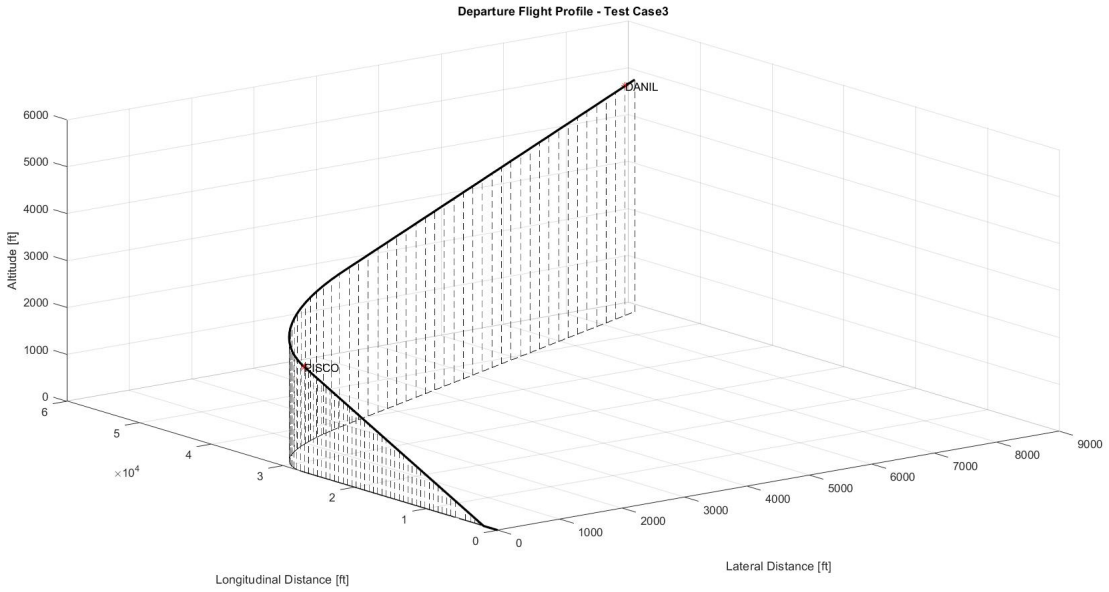

Figure 6.5: Flight path - Test case 3 with turning radius of 20.000ft

6.3 Noise Levels At The Observer

In this section is obtained the noise at the fixed receiver located at EXPO $(38°46'09.5"N 9°05'32.9"W)$ during the aircraft departure from Montijo. The simulation parameters are the ones refered in section 4.7 from GFPE's validation.

According to previous studies [13] it is possible to verify that limiting the frequency range of the simulations to a maximum frequency $4kHz$ produces the same results as the entire $1/3$ -octave band, as the variations in the SEL at the receiver are negligible up to $10kHz$.

This phenomenon is due to the absorption of the highest frequencies by the atmosphere which attenuates the corresponding pressure levels. The figure 6.6 displays the SPL and the distance between the observer and the aircraft as functions of time where the distance between the source and the receiver is the governing parameter of the SPL. Each test case considered the three different types of atmosphere (homogeneous, downward refracting and upward refracting) in order to perceive its influence in the noise levels at the observer.

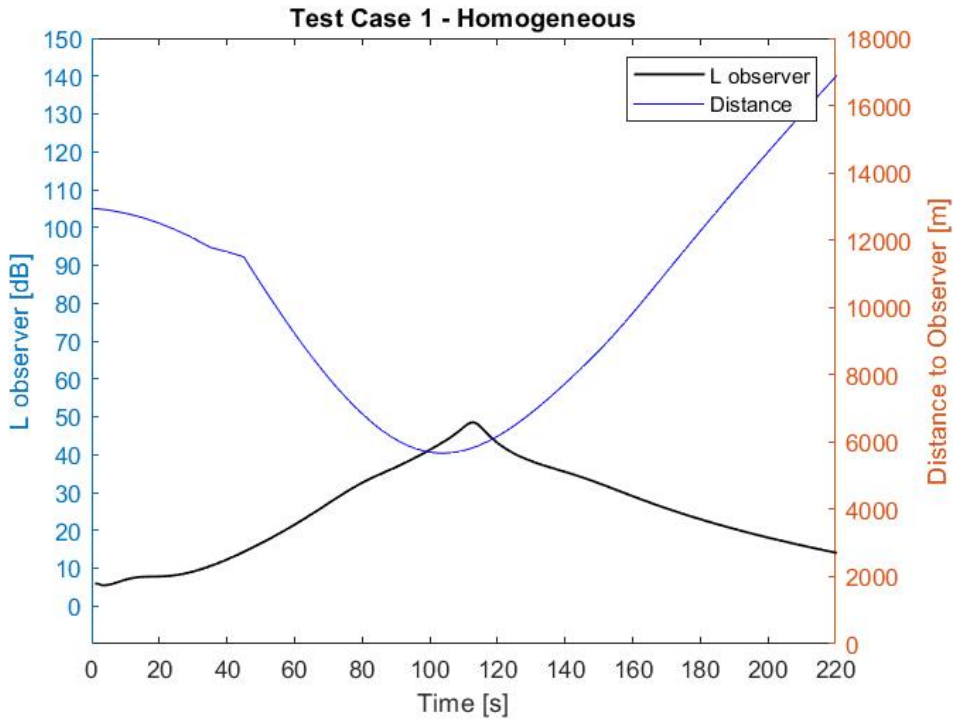

Figure 6.6: OASPL levels and range time history for the test case 1 departure in a homogeneous atmosphere

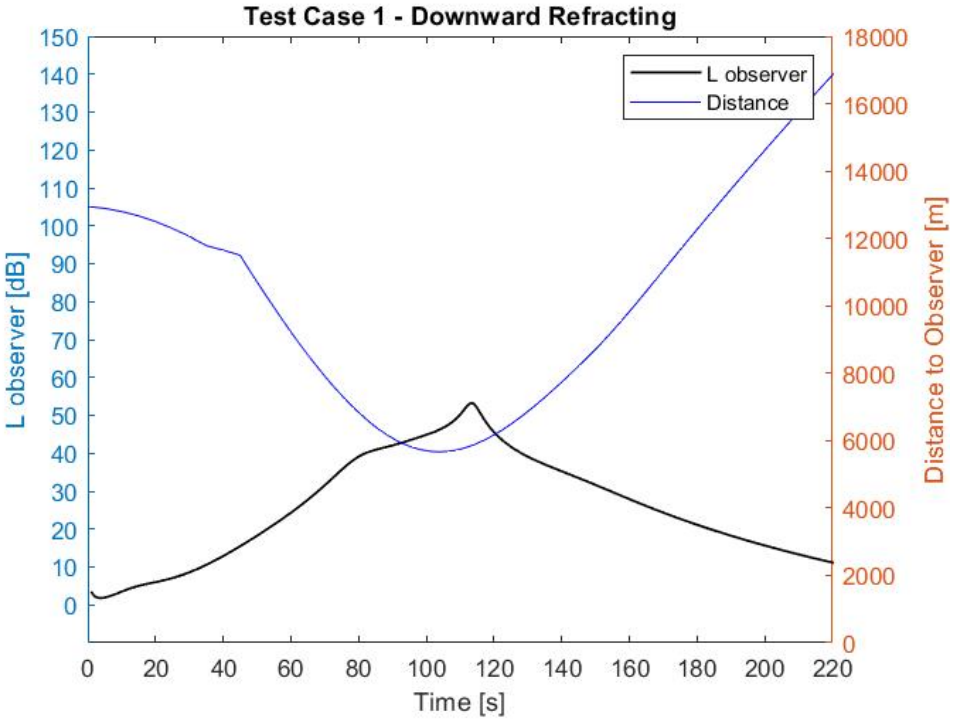

Figure 6.7: OASPL levels and range time history for the test case 1 departure in a downward refracting atmosphere

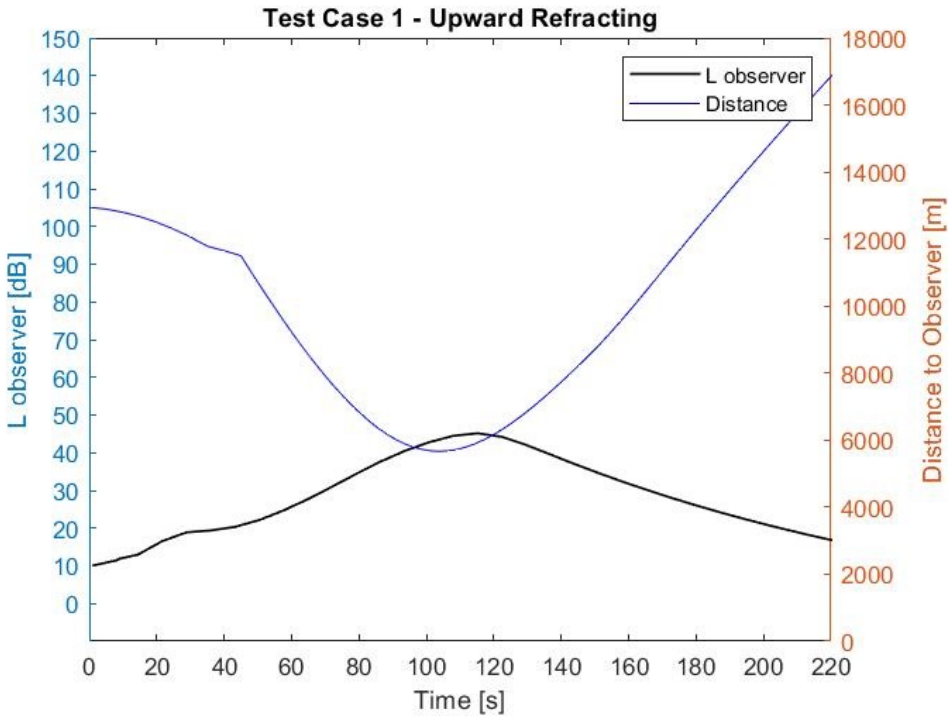

Figure 6.8: OASPL levels and range time history for the test case 1 departure in an upward refracting atmosphere

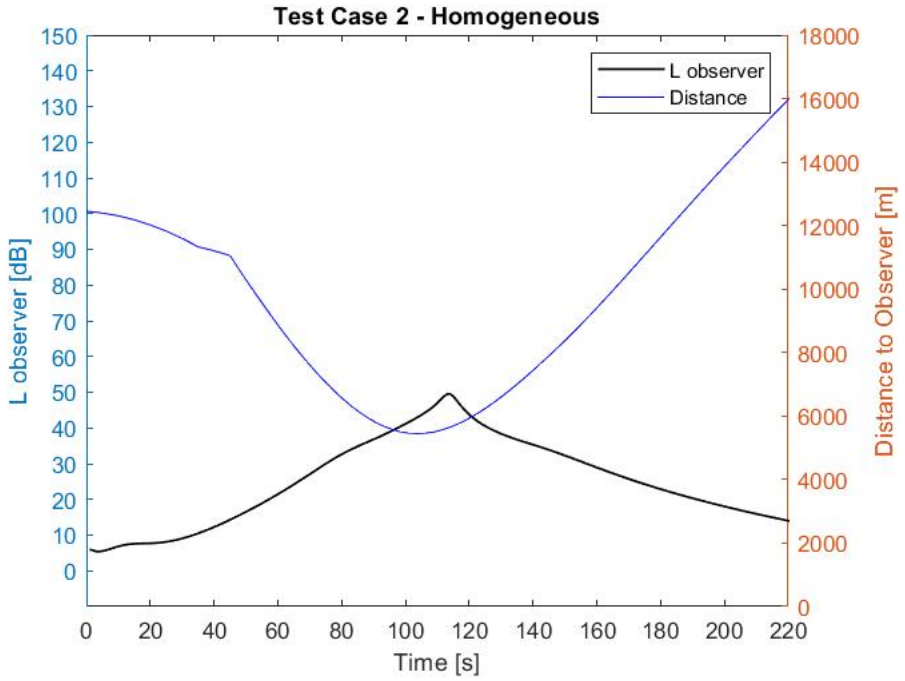

Figure 6.9: OASPL levels and range time history for the test case 2 departure in a homogeneous atmosphere

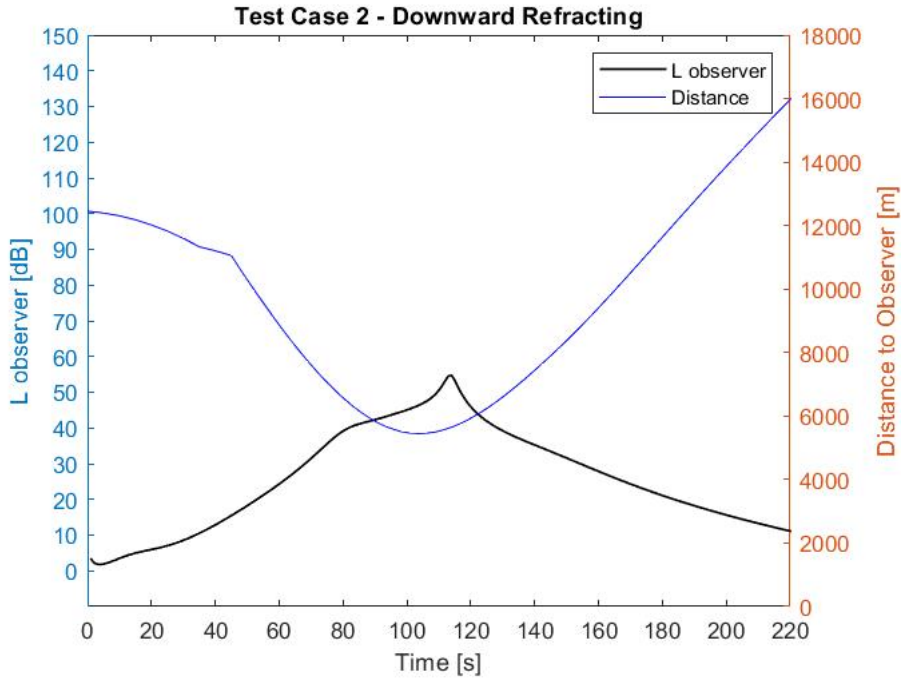

Figure 6.10: OASPL levels and range time history for the test case 2 departure in a downward refracting atmosphere

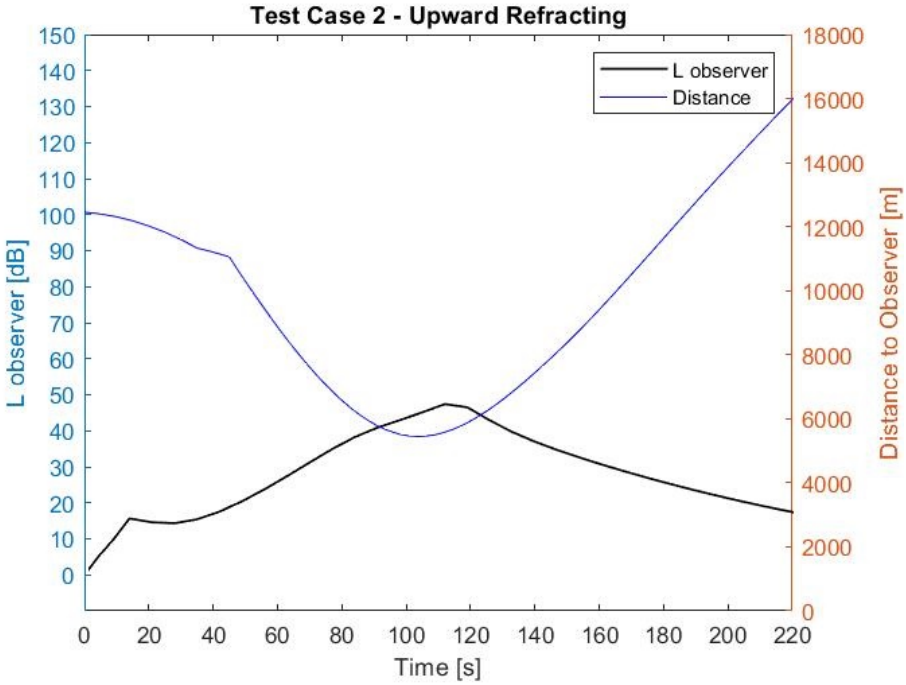

Figure 6.11: OASPL levels and range time history for the test case 2 departure in an upward refracting atmosphere

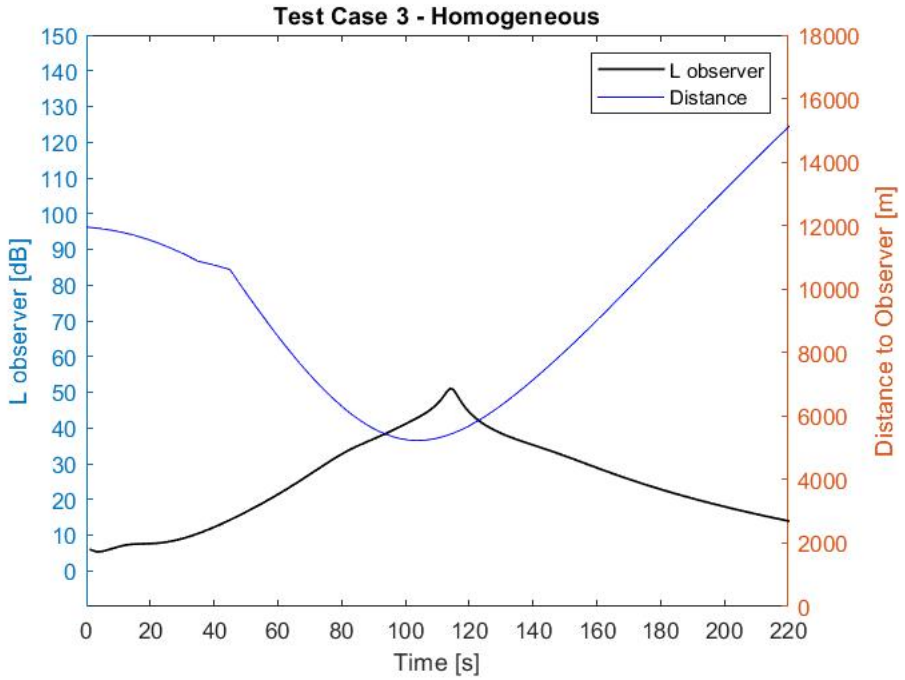

Figure 6.12: OASPL levels and range time history for the test case 3 departure in a homogeneous atmosphere

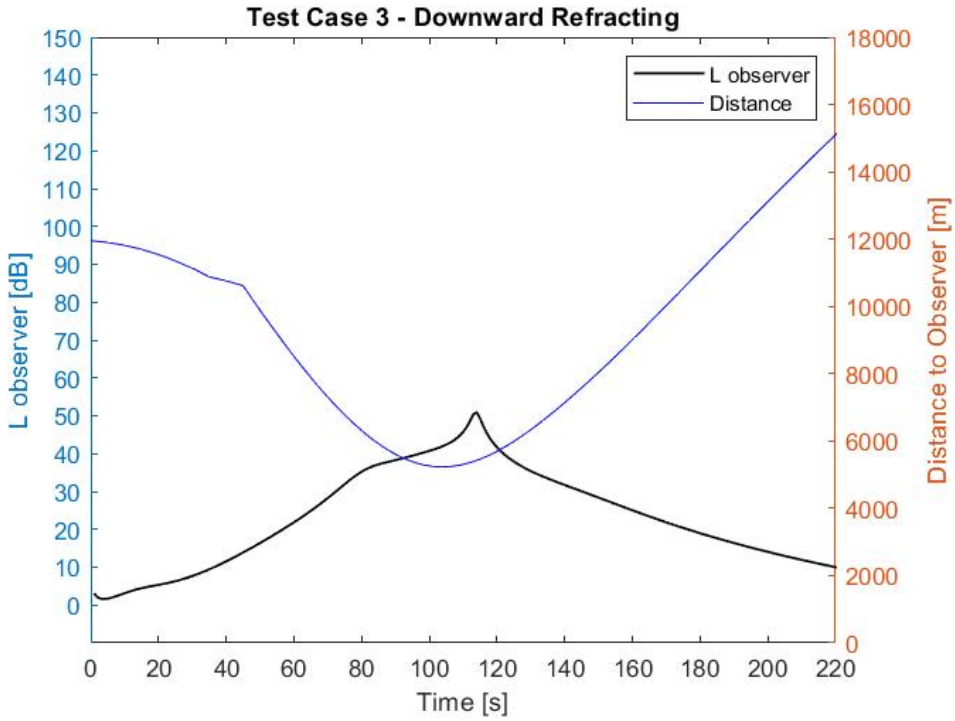

Figure 6.13: OASPL levels and range time history for the test case 3 departure in a downward refracting atmosphere

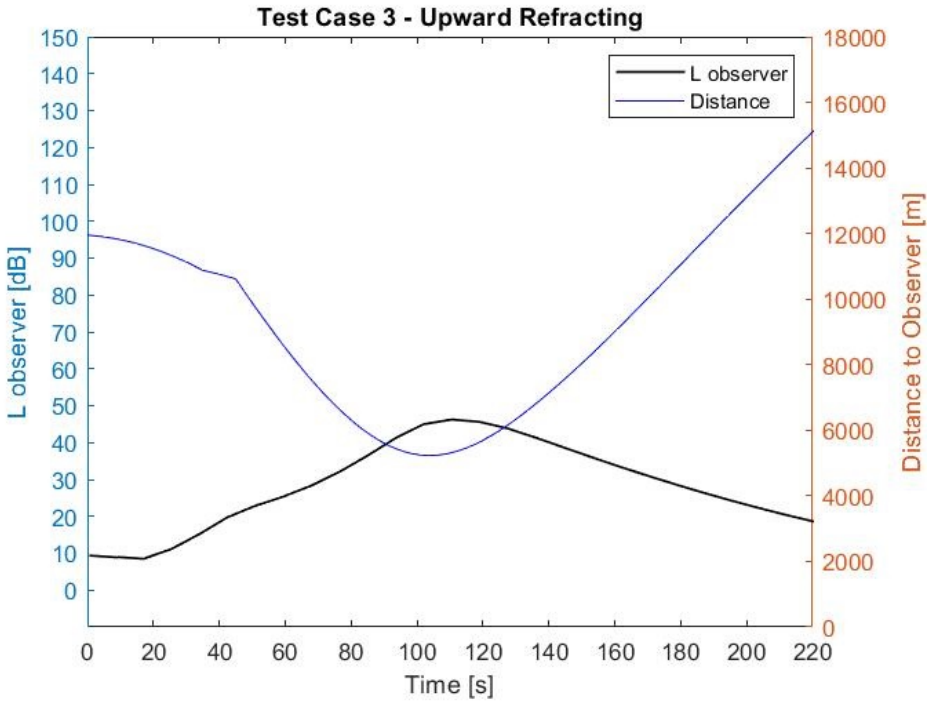

Figure 6.14: OASPL levels and range time history for the test case 3 departure in an upward refracting atmosphere

The results suggest that there are very little differences for the three test case trajectories and that is because the three have the turning zone situated at the same location in which the distance is minimum to the observer. This results in approximately the same range between the source and the receiver and therefore it is not expected that the noise levels vary that much.

We can also notice that the maximum noise levels at the observer have a similar evolution for the homogeneous and the downward refracting atmosphere and that is supported by the fact of the distance being large where the noise levels are not that much changed. Also for every plot we can see a displacement between the minimum distance and the maximum noise which has the value of the time that sound needs to propagate in the atmosphere. In other words, when the aircraft is at its nearest position from the receiver, it takes a certain time to travel and therefore the maximum noise level its just perceived at the receiver after a while, corresponding to the time that the sound takes to travel along the distance between them for a constant sound speed.

In the test case 1 trajectory the maximum noise level at the observer is 50 dB for the homogeneous atmosphere while for the downward refracting atmosphere is 53 dB. This small change is due to the fact that the sound waves are bend downward through out its path and this allows to reach higher levels for the same travelled distance, however since the distance is very large the difference is very little and probably unnoticed by the observer. For the upward refracting atmosphere simulation the noise levels are more attenuated than in the other types and only reach a maximum level of approximately 46 dB

with a much more smooth evolution along the time history. Therefore it is possible to conclude that an upward refracting atmosphere is favorable for attenuating noise levels generated by aircraft departures.

For the test case 2 and 3 trajectories the noise levels perceived by the observer are in the same range of values that the test case 1 and this suggests that the turning radius after the PISCO zone does not influence much the noise levels at the observer since that the difference of the distances between the observer and the source are very small when compared to the overall distance that the sound travels.

From a practical point of view it is possible to claim that taking into account the predicted levels of noise at the specified observer, the Montijo's future airport won't generate significant levels of noise at the riverside zone of Lisbon since these noise levels are similar to those generated in a normal conversation. Taking into account that in this zone there is a considerable ammount of cars traffic and that it also has a large train station. it is expected that the normal noise levels in this zone during the day reach near 80 dB, according to the noise map of Lisbon made available in the town hall website. We can then affirm that the noise generated by an aircraft departure is almost or totally unnoticed at the observer location.

In order to validate this results a comparison was made with a previous study of noise abatement procedures [13] and it was sucessfully achieved a validation for the evolution of the sound levels at the observer and also for the values obtained and therefore the GFPE model may be used to predict aviation noise for the departure of an aircraft.

In order to understand better the influence and weight of different individual frequencies in the overall sound pressure level, it is presented the SPL results for three different frequencies of the 1/3 octave band spectrum at the observer characterized in this section. The chosen frequencies assume the values of f=63 Hz, f=500 Hz and f=2000 Hz and the simulations were executed for the same parameters of the previous test cases and refer to the trajectory of the test case 1 for a homogeneous atmosphere.

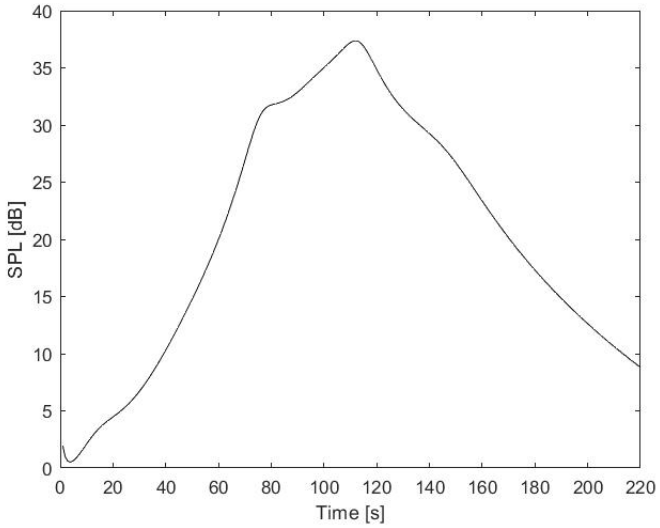

Figure 6.15: SPL for f=63 Hz for test case 1 trajectory

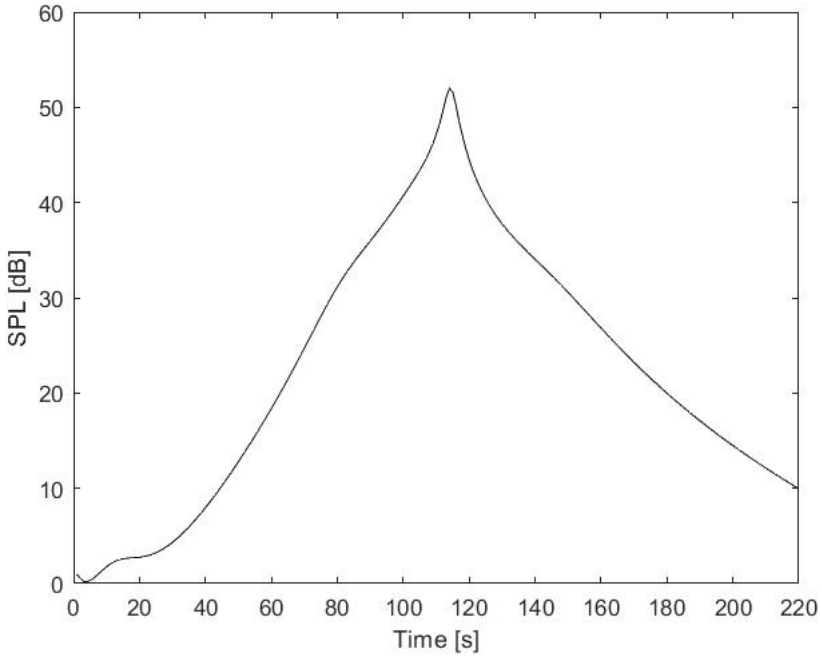

Figure 6.16: SPL for f=500 Hz for test case 1 trajectory

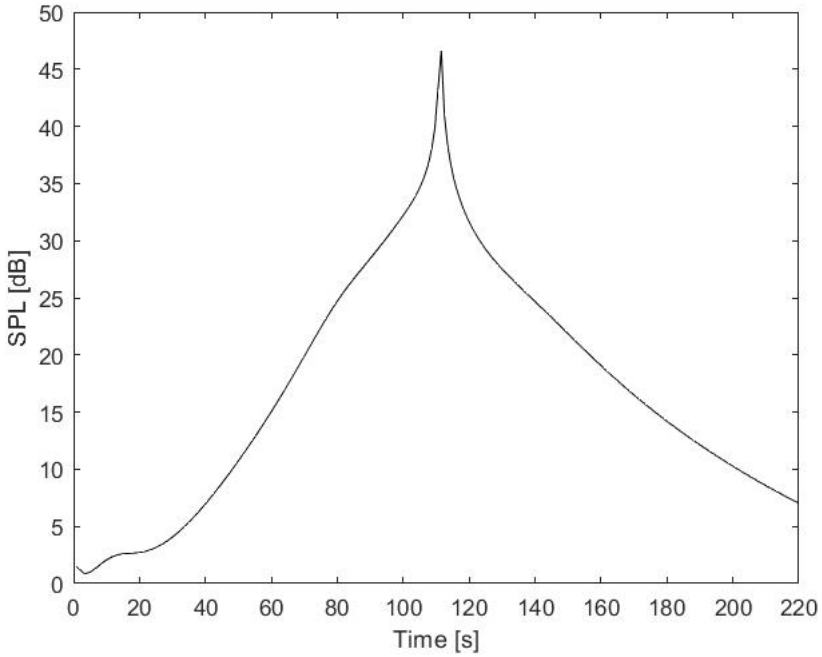

Figure 6.17: SPL for f=2000 Hz for test case 1 trajectory

Based on the three plots of the SPL in function of time, it is possible to conclude that for the low frequencies, in this specific case f=63 Hz, they are not that much absorbed by the atmosphere and therefore maintain approximately the same levels of intensity for a longer period of time. In the figure 6.15 is possible to notice the wider shape of the SPL evolution for the frequency of f=63Hz when compared to the two other frequencies.

Increasing the frequency to f=500 Hz the maximum sound intensity level change singnificantly and the SPL evolution starts to get a narrow shape, suggesting that the sound for this frequency undergo more atmospheric absorption than the previous frequency of f=63 Hz.

For the frequency of f=2000 Hz, a peak shape characterizes the evolution of the SPL as well as a decrease of the maximum value at the observer of approximately -4 dB when compared to the frequency of f=500 Hz. This is in agreement with the outdoor sound propagation literature that predict that high frequencies are more attenuated due to atmosphere properties at the same time that the distance between the observer and the source is the governing parameter for the SPL level citeSalomons.

Finally, the Sound Exposure Level (SEL) was obtained according to the equation 5.13, which accounts the integration of the SPL curve during the aircraft departure procedure. As the relevant sound energy for the 10dB down integration is concentrated around the maximum SPL value, only a small part of the aircraft's trajectory is considered in the calculations due to the rapid evolution of the SPL curve at the proximity of the maximum SPL value. An aircraft noise event can be described by its observed level-time-history L(t) as shown below.

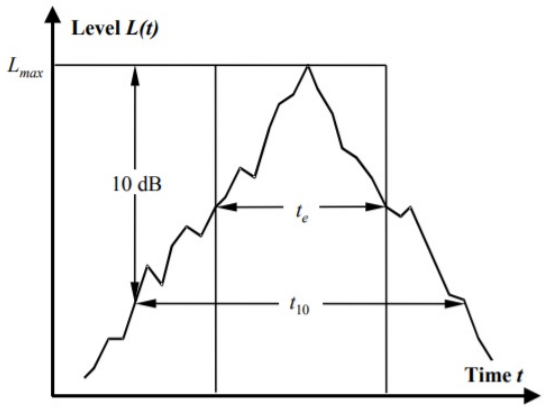

Figure 6.18: Level-time-history of a noise event and noise-related parameters [8]

Where L_{max} is the maximum sound level, t_e the effective duration that contains the same sound energy as the noise event and t_{10} the time period during which the sound level lies within 10 dB of the maximum sound level L_{max}.

The values of sound exposure level (SEL) and L_{max} for each trajectory test case and each atmosphere type are presented below.

	Test Case 1		
	Homogeneous Atmosphere	Downward refracting	Upward refracting
SEL (L_{AE})	55.3 dB	57.8 dB	54.2 dB
L_{max}	49.5 dB(A)	53.9 dB(A)	46.7 dB

Figure 6.19: L_{max} and L_{AE} for Test Case 1

	Test Case 2		
	Homogeneous Atmosphere	Downward refracting	Upward refracting
SEL (L_{AE})	56.2 dB	58.8 dB	55.1 dB
L_{max}	51.3 dB(A)	54.4 dB(A)	47.9 dB

Figure 6.20: L_{max} and L_{AE} for Test Case 2

	Test Case 3		
	Homogeneous Atmosphere	Downward refracting	Upward refracting
SEL (L_{AE})	57.8 dB	59.1 dB	55.4 dB
L_{max}	51.9 dB(A)	54.8 dB(A)	48.4 dB

Figure 6.21: L_{max} and L_{AE} for Test Case 3

From the presented tables one can conclude that in a general way the sound exposure level is increased by a downward refracting atmosphere at the same time that the maximum noise level is too. For low elevation angles between the source and the receiver as is the case in all trajectories, the diference in between an upward and downward refracting atmosphere is larger, and less than 4 dB of difference. We can also notice that the wider the trajectory is, the higher the value of L_{max} and consequently the higher the value of the SEL is.

Regarding the point that is the interest of the general population that live nearby the zone of EXPO where the observer is located to have the minimum possible levels of noise for a Montijo's airport departure, the results suggest that the departure trajectory should have the characteristics of the Test Case 1 since as it is predicted, less noise reaches the observer.

7

Final Conclusions

Throughout this thesis, several challenges were faced. Starting with the mathematical complexity of the acoustic equations and with the challenging difficulty of its computational implementation to the combination of it with the aircraft trajectory planning and the associated calculations. By taking advantage from the noise prediction tools previously developed in other studies it was possible to obtain computational results that gives us a starting base for further realistic noise models with better accuracy.

The numerical scheme used to calculate sound propagation in the atmosphere were the Green's Function Parabolic Equation (GFPE) method and the algorithm used to predict the aircraft trajectory during a possible departure at Montijo aerodrome was taken from ECAC Vol.I and Vol.II procedures which were then incorporated through a Matlab program. These methods were combined to obtain a time history of the noise values at the fixed observer, located in the EXPO zone, along the departure of the aircraft. The GFPE code was tested in three distinct atmospheric conditions and the results obtained from the simulations were consistent with the benchmark data and with the previous studies about this theme.

The results obtained in this thesis include multiple simplifications that should be considered, as for example the exclusion of turbulence and wind, however, for the purpose of this thesis, it was possible to take a notion of how much predicted impact the noise produced by an aircraft takes on a person while within a radius of considerable large distance. The obtained results made possible to take some conclusions, being briefly concluded that for an Airbus A320 with motors CFM565, a single individual would perceive a very low noise level during a Montijo's airbase departure, and therefore, the impact generated for the Oriente living zone is predicted to be insignificant when compared to the noise levels already existing.

For a more realistic and accurate study, several developments should be included as for example the consideration of a turbulent atmosphere and also atmospheric wind. The ground surface should be developed in detail in order to be possible to simulate noise barriers and other topographic features and obstacles, and should even be considered different ground materials not forgeting the aircraft cinematics, which also play a very important role, and which should be included with much more detail in the algorithm to allow to obtain a more realistic flight path.

Bibliography

[1] Erik Salomons. *Computational Atmospheric Acoustics*. Springer Netherlands, 1st edition, 2001.

[2] DOSITS. Discovery of sound in the sea. https://dosits.org/science/advanced-topics/cylindrical-vs-spherical-spreading/,[accessed at 2020-03-24].

[3] Neal Ewanleifoh. Noise Control Outdoors. *The Department of Architecture Federal University of Technology Akure*, 2014.

[4] André Oliveira. Msc thesis on: The effect of wind and turbulence on sound propagation in the atmosphere. 2012.

[5] ECAC-European Civil Aviation Conference. Standard Method of Computing Noise Contours around Civil Airports. Technical report, 2016.

[6] Ralf Mayer. A flight trajectory model for a pc-based airspace analysis tool. 2003.

[7] João Mendonça, Manuel Araújo. Estudo de Rotas Alternativas e Altitudes - Pistas 01 e 19, 2018.

[8] ECAC-European Civil Aviation Conference. Standard Method of Computing Noise Contours around Civil Airports. Technical report, 2016.

[9] Keith Attenborough. Benchmark cases for outdoor sound propagation models. *The Journal of the Acoustical Society of America*, 97, 1995.

[10] Eric Heller. "Why you hear what you hear: An experiential approach to sound, music, and psychoacoustics". *Princeton University Press*, 2012.

[11] Roy Deavenport Frederick DiNapoli. Computer models of underwater acoustic propagation. *Naval Underwater Systems Center*, 1980.

[12] Yannick Gabillet. Application of the gaussian beam approach to sound propagation in the atmosphere: Theory and experiments. *The Journal of the Acoustical Society of America*, 93, 1993.

[13] André de Sousa. Msc thesis on :flight path optimization for noise reduction in the vicinity of airports. 1, 2015.

[14] Siemens. Sound Transmission Loss - Determining the Acoustic Properties of Materials Solution Brief. https://community.sw.siemens.com/s/article/sound-transmission-loss, [accessed at 2020-03-24].

[15] Keith Attenborough. Sound propagation close to the ground. *Annual Review of Fluid Mechanics*, 34, 2002.

[16] Michael White Kenneth Gilbert. Application of the parabolic equation to sound propagation in a refracting atmosphere. *The Journal of the Acoustical Society of America*, 85, 1989.

[17] Herman Feshbach Philip Morse. *Methods of Theoretical Physics, Part I*, volume 1. McGraw-Hill Science/Engineering/Math, 1953.

[18] Allen Pierce. Acoustics: An introduction to its physical principles and applications. *Springer*, 22, 1981.

[19] Kenneth Gilbert. A fast green's function method for one-way sound propagation in the ocean. *The Journal of the Acoustical Society of America*, 95, 1994.

[20] Vladimir Ostashev, Michael Muhlestein, and David Wilson. Extra-wide-angle parabolic equations in motionless and moving media. *The Journal of the Acoustical Society of America*, 2019.

[21] Fred Tappert. The parabolic approximation method. *Wave Propagation and Underwater Acoustics*, 1977.

[22] John Buck Alan Oppenheim, Ronald Schafer. *Discrete-Time Signal Processing*. Prentice-Hall Signal Processing Series. Prentice Hall, 2nd ed edition, 1999.

[23] D. Champeney. *Fourier transforms and their physical applications*. Techniques of physics 1. Academic Press, 1973.

[24] S. Teukolsky W. Vetterling W. Press, B. Flannery. *Numerical Recipes Example Book FORTRAN*. Cambridge University Press, 5th printing edition, 1986.

[25] S. Johnson M. Frigo. The design and implementation of fftw3. *Proceedings of the IEEE*, 93, 2005.

[26] James Cooley and John Tukey. An algorithm for the machine calculation of complex fourier series. *Mathematics of Computation*, 19, 1965.

[27] D. Thomson and N. Chapman. A wide angle split-step algorithm for the parabolic equation. *The Journal of the Acoustical Society of America*, 74, 1983.

[28] David Swanson Jennifer Cooper. Parameter selection in the green's function parabolic equation. *Applied Acoustics*, 68, 2007.

[29] Oleksandr Zaporozhets. *Aircraft Noise Models for Assessment of noise around Airports - Improvements and Limitations*. 2016.

[30] Janito Permanande. Msc thesis on: Optimization of rnav departure trajectories with respect to environmental criteria. *Outdoor Propagation Acoustics*, 1, 2016.

[31] Força Aérea Portuguesa. *https://www.emfa.pt/unidade-19-base-aerea-n-6*, [accessed at 2020-08-01].

[32] LPMT - Montijo Air Base N6, PT - Airport Great Circle Mapper. *http://www.gcmap.net/airport/LPMT*, [accessed at 2020-07-16].

[33] ICAO-International Civil Aviation Organization. Rules of the Air Annex 2 to the Convention on International Civil Aviation International Standards . Technical report, 2016.

[34] ICAO-International Civil Aviation Organization. Air Traffic Services Annex 11 to the Convention on International Civil Aviation, International Standards and Recommended Practices Air Traffic Control Service Flight Information Service Alerting Service. Technical report, 2001.

[35] Danger Area - SKYbrary Aviation Safety. *https://www.skybrary.aero/index.php/Danger_Area*, [accessed at 2020-08-15].

GFPE Test Cases & Benchmark Results

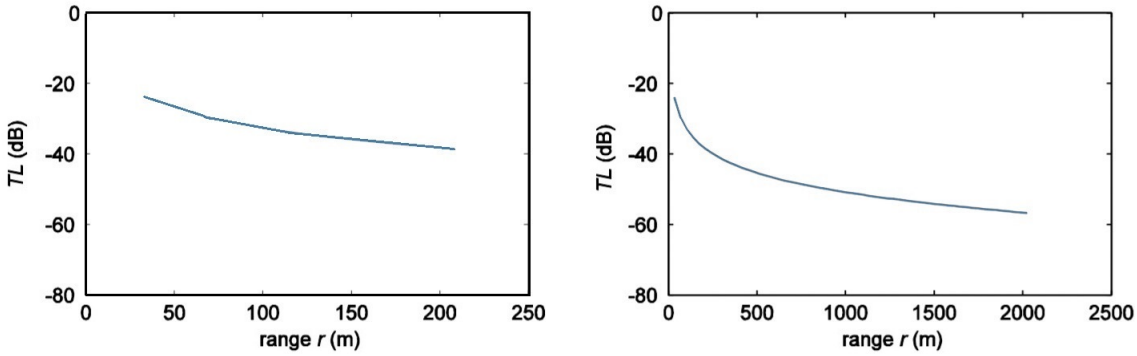

Figure A.1: Transmission loss for 10Hz - Test case 1

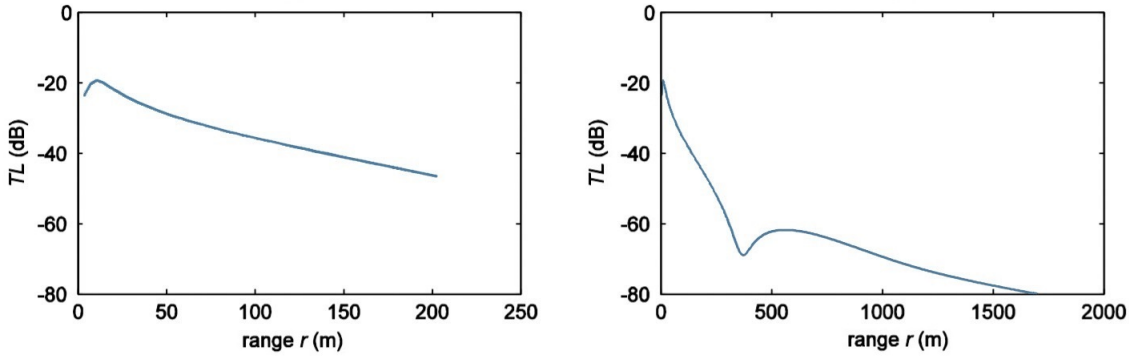

Figure A.2: Transmission loss for 100Hz - Test case 1

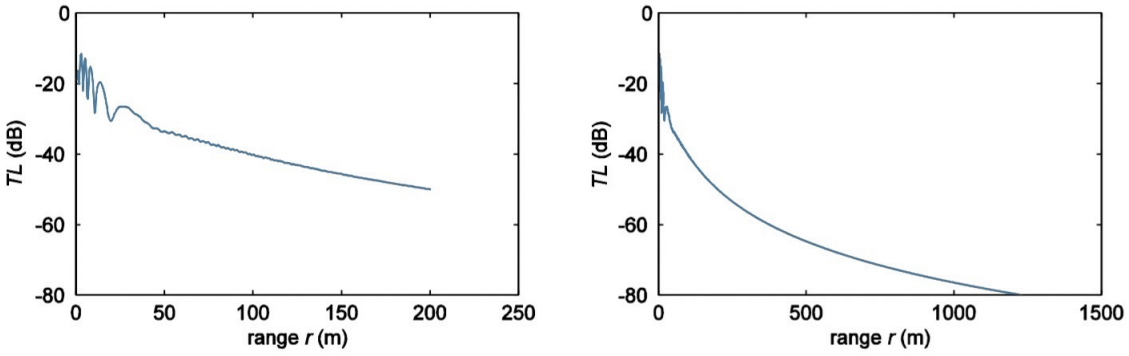

Figure A.3: Transmission loss for 1000Hz - Test case 1

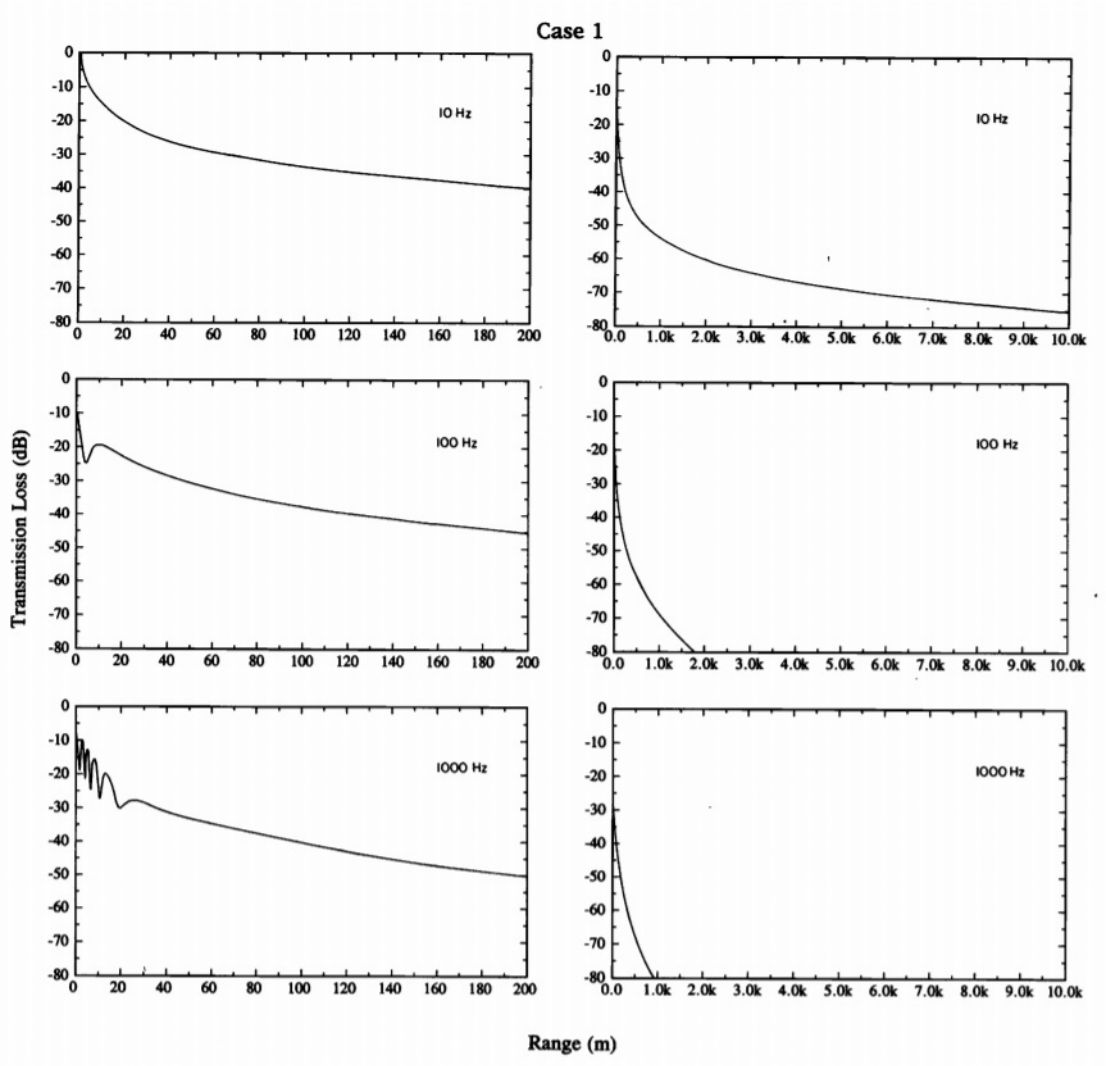

Figure A.4: Benchmark result for test case 1 [9]

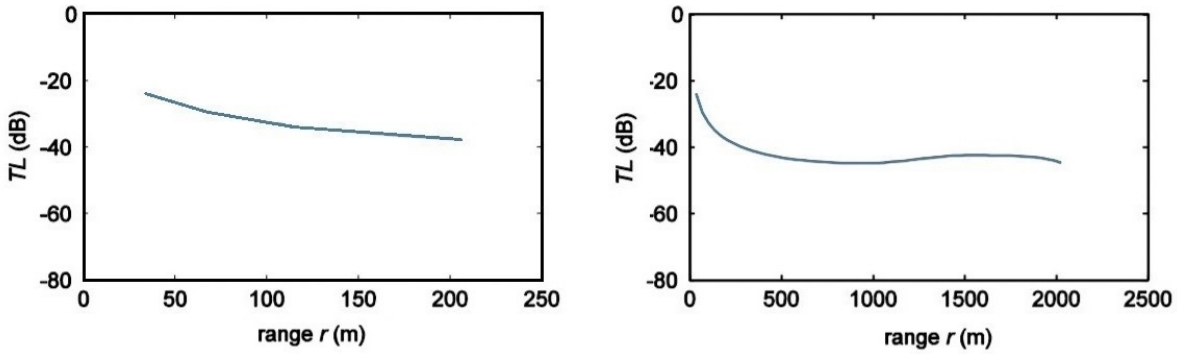

Figure A.5: Transmission loss for 10Hz - Test case 2

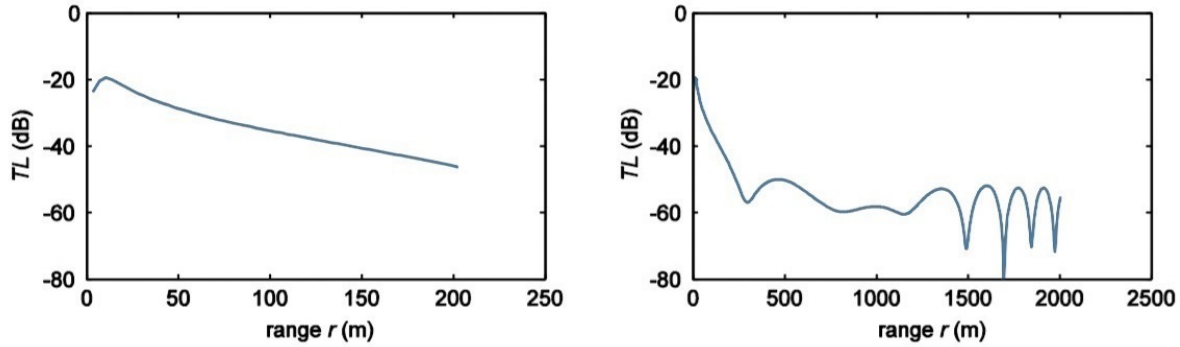

Figure A.6: Transmission loss for 100Hz - Test case 2

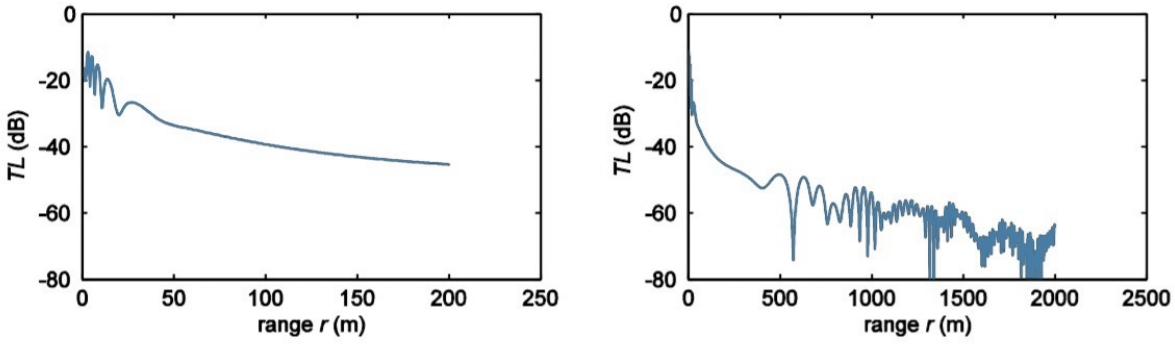

Figure A.7: Transmission loss for 1000Hz - Test case 2

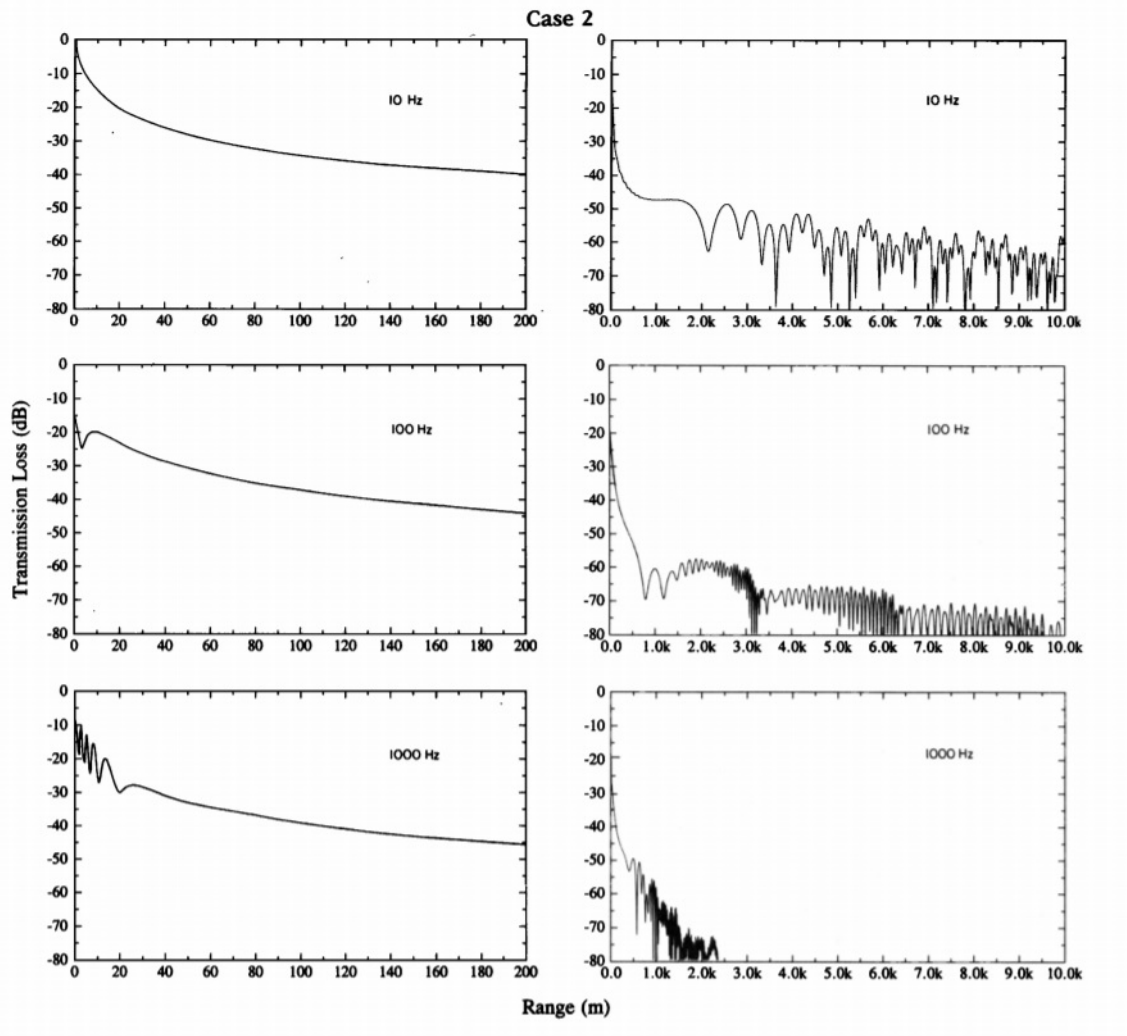

Figure A.8: Benchmark result for test case 2 [9]

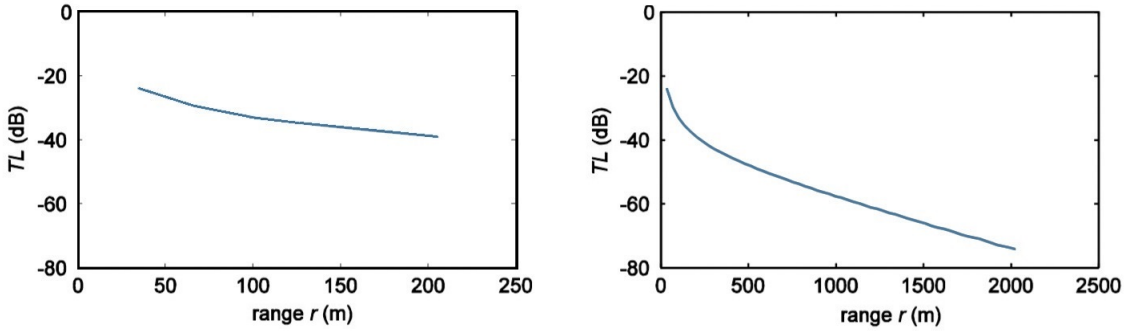

Figure A.9: Transmission loss for 10Hz - Test case 3

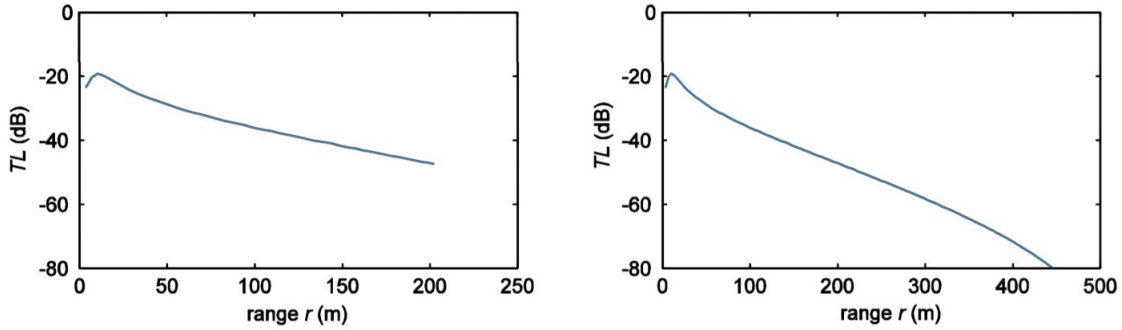

Figure A.10: Transmission loss for 100Hz - Test case 3

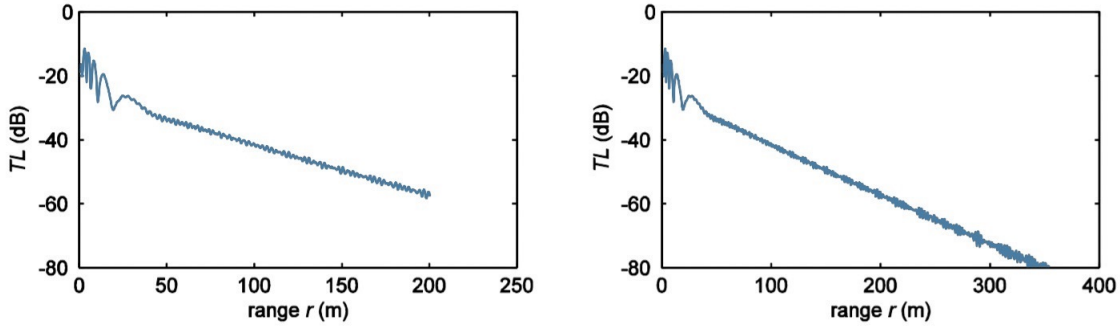

Figure A.11: Transmission loss for 1000Hz - Test case 3

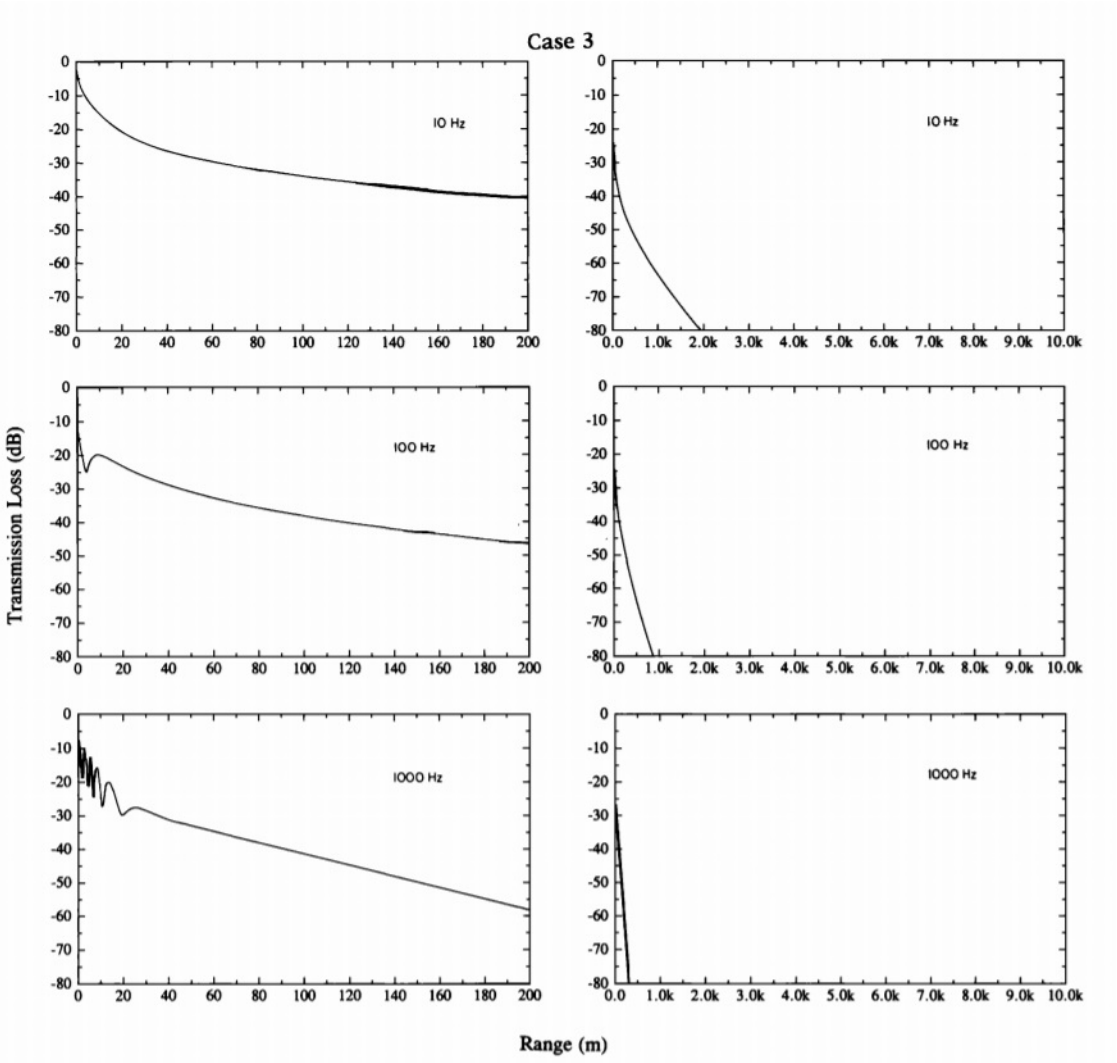

Figure A.12: Benchmark result for test case 3 [9]

B

EWAPE Results

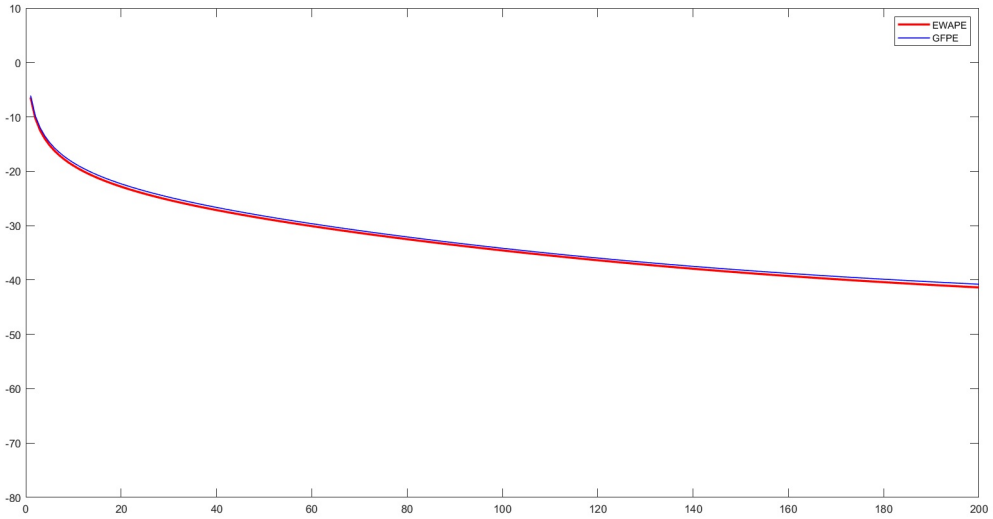

Figure B.1: EWAPE and GFPE for a f=10Hz and R=200m

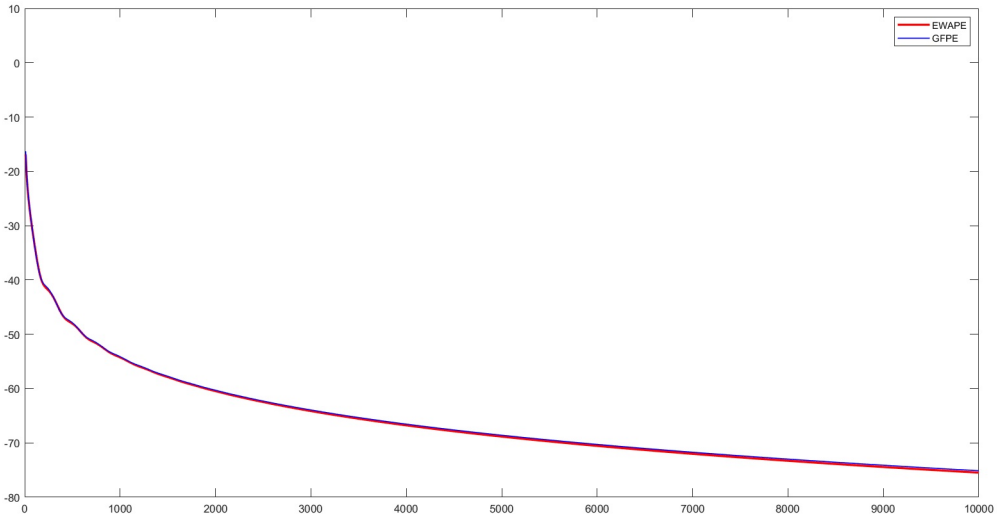

Figure B.2: EWAPE and GFPE for a f=10Hz and R=10km

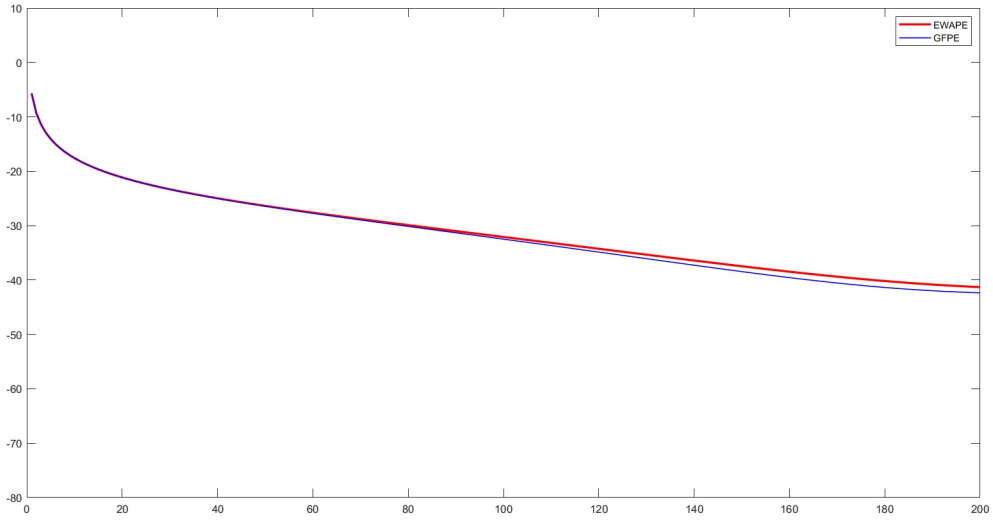

Figure B.3: EWAPE and GFPE for a f=100Hz and R=200m

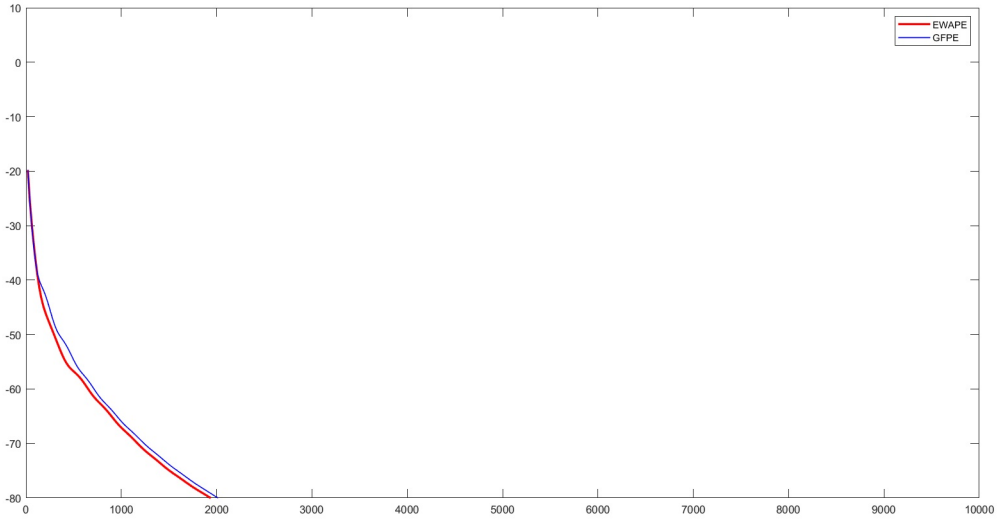

Figure B.4: EWAPE and GFPE for a f=100Hz and R=10km

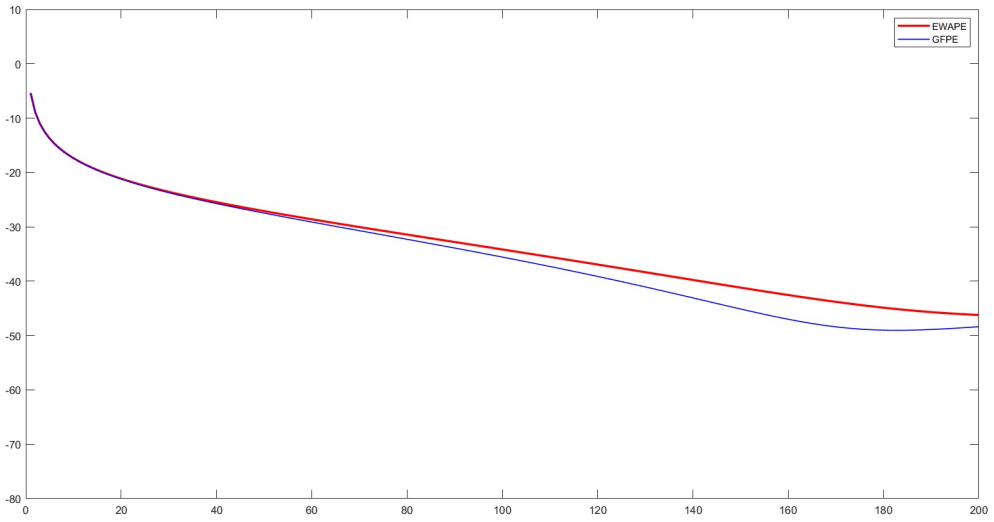

Figure B.5: EWAPE and GFPE for a f=1000Hz and R=200m

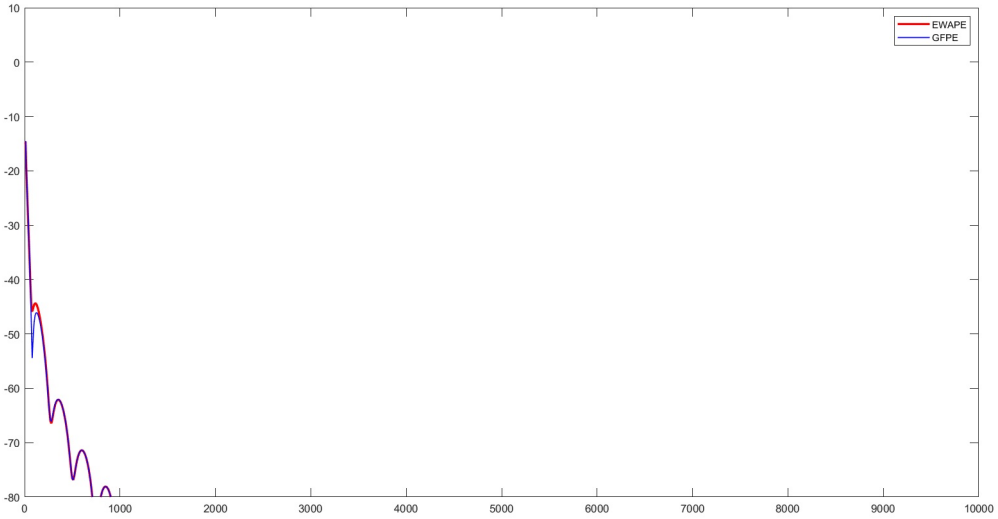

Figure B.6: EWAPE and GFPE for a f=1000Hz and R=10km